

Aging of Alloy 617 at 650 and 750°C

Julian Benz
Thomas Lillo
Richard Wright

January 2013



The INL is a U.S. Department of Energy National Laboratory
operated by Battelle Energy Alliance

DISCLAIMER

This information was prepared as an account of work sponsored by an agency of the U.S. Government. Neither the U.S. Government nor any agency thereof, nor any of their employees, makes any warranty, expressed or implied, or assumes any legal liability or responsibility for the accuracy, completeness, or usefulness, of any information, apparatus, product, or process disclosed, or represents that its use would not infringe privately owned rights. References herein to any specific commercial product, process, or service by trade name, trade mark, manufacturer, or otherwise, does not necessarily constitute or imply its endorsement, recommendation, or favoring by the U.S. Government or any agency thereof. The views and opinions of authors expressed herein do not necessarily state or reflect those of the U.S. Government or any agency thereof.

Aging of Alloy 617 at 650 and 750°C

Julian Benz, Thomas Lillo, and Richard Wright

January 2013

**Idaho National Laboratory
Materials Science and Engineering
Idaho Falls, Idaho 83415**

<http://www.inl.gov>

**Prepared for the
U.S. Department of Energy
Office of Nuclear Energy
Under DOE Idaho Operations Office
Contract DE-AC07-05ID14517**

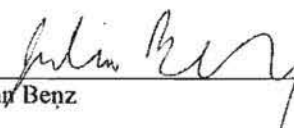
Materials Science and Engineering

Aging of Alloy 617 at 650 and 750°C

INL/EXT-12-27974

January 2013


Approved by:



Julian Benz

1/7/2013

Date



Tom Lillo

1/7/2013

Date



Richard Wright

1/7/2013

Date

ABSTRACT

Alloy 617 has been selected as the primary candidate for heat exchanger applications in advanced reactors. For the VHTR this application could require extended service up to a reactor outlet temperature of 950°C. A key hurdle to using this alloy in the VHTR heat exchanger application is qualifying the alloy for Section III of the ASME Boiler and Pressure Vessel Code. In order to Code qualify the material it is necessary to characterize the influence of long term aging on the mechanical behavior. Aging at relatively low temperatures, 650°C in particular, is thought to result in significantly reduced ductility and impact properties. The primary focus of this report is on the influence of aging at 650°C on microstructure and properties of Alloy 617; additional aging effects at higher temperature will be included for comparison.

Alloy 617 has been aged at 650°C for times up to 5300 hours. The microstructure after aging has been characterized using optical and transmission electron microscopy (TEM). The Alloy 617 plate shows an evolution of microstructure even after aging for the relatively short period of 200 hours at both 650 and 750°C. This observation is consistent with the TTT diagram for Alloy 617 which shows that $M_{23}C_6$, M_6C , and γ' will start precipitating in as little as one hour at these temperatures. Comparing the as-received microstructure to that of aged material, both the 650 and 750°C show a similar amount of carbide precipitation. At both aging temperatures, the majority of carbides are intragranular and there is no indication of carbide redistribution or precipitation directly on the grain boundaries. The carbides appear to partly retain the cell structure seen in the as-received material in the banding regions. It has been determined that in addition to carbides, a significant volume fraction of γ' phase (Ni_3Al,Ti) is formed at these temperatures. The $Ni_3(Al,Ti)$ phase is only observable using TEM. The size and morphology of the carbides and γ' continue to evolve with increasing aging time at both temperatures.

After aging at 650°C the room temperature yield and tensile strength increase with increasing time. The ductility decreases from 62% in the solution annealed material compared to 42% for material aged for 5300 hours. Aging has a more significant influence on the impact properties of Alloy 617 compared to the tensile properties. The room temperature Charpy energy for solution annealed Alloy 617 is above 150J. Aging for 200 hours results in a decrease in Charpy energy to 95J and 75J for aging at 750 and 650°C, respectively. Increasing the aging time to 5300 hours at 650°C results in further reduction in Charpy energy to approximately 60J.

Precipitation and coarsening kinetics of γ' has been studied in detail after aging at both 650 and 750°C. It has been found that the presence of this phase affects the creep properties of Alloy 617 at 750°C. A threshold stress model is necessary to account for the creep behavior at this temperature, with a value for $\sigma_{\text{threshold}}$ of approximately 65MPa. Above this temperature there is no formation of γ' and the creep properties can be modeled with a conventional Norton Law formulation with no threshold stress.

CONTENTS

ABSTRACT.....	iv
ACRONYMS.....	x
Introduction.....	1
Background.....	2
Results and Discussion	9
Optical Microstructure.....	9
As-Received Microstructure	9
Microstructure After Aging 200 Hours.....	9
Microstructure After Aging 5300 Hours.....	11
Mechanical Testing on Aged Material	14
Tensile Results	14
Charpy Impact Energy	16
Crack Growth.....	17
Gamma Prime Particle Size Analysis.....	19
Materials Analyzed	19
Results and Discussion.....	21
Analysis of Creep Properties	25
Conclusions.....	28
References.....	29

FIGURES

Figure 1. Time-temperature-transformation (TTT) diagram for long term aging of Alloy 617. ³	4
Figure 2. J-R Curve for solution annealed Alloy 617 at 700°C.	4
Figure 3. (a) Values of J_0 and (b) tearing modulus for Alloy 617, as received (temperature in Kelvin).	5
Figure 4. Room temperature CVN energy of Alloy 617 after thermal exposure.	6
Figure 5. CVN energy of aged Alloy 617 measured at room temperature and aging temperature.	6
Figure 6. Load vs. crack mouth opening displacement record and a plot of J versus Δa (crack extension) for a 0.5T compact fracture toughness test performed at room temperature.	8
Figure 7. Charpy impact energies for solution annealed and aged Alloy 617 tested at temperatures from ambient to 900°C.	8
Figure 8. Highest observed CVN impact energies of solution annealed and aged Alloy 617.	8
Figure 9. Optical microstructure of the as-received Alloy 617 material at 100x magnification and oriented with the rolling direction in the y-axis. The as-received material shows significant banding which is apparent in the image.	9

Figure 10. Image showing the optical microstructure of plate aged at 650°C for 200 hours. The orientation and magnification are the same as in Figure 9.	10
Figure 11. Microstructure of the plate aged at 750°C for 200 hours. The orientation and magnification are the same as in Figure 9.	10
Figure 12. Two images of the microstructure from plate aged at 750°C for 200 hours. (a) shows the serrated nature of the grain boundaries caused by grain movement in a small region of the plate and (b) shows the migration of carbides to regions directly adjacent.....	12
Figure 13. Microstructure of the plate after aging for 5300 hours at 650°C. The orientation and magnification are the same as in Figure 9.	12
Figure 14. Optical microstructure of the plate after aging at 750°C for 5300 hours. The orientation and magnification are the same as in Figure 9.....	13
Figure 15. High magnification optical micrograph of the material aged at 750°C for 5300 hours. Clusters or sunburst patterns of carbides are apparent in this image.....	13
Figure 16. Room temperature tensile test results of the as-received material and material aged at 650°C for various times.....	15
Figure 17. Tensile test results for material aged at 650°C for various times and a test temperature of 650°C. The as-received material tensile results for comparison are at room temperature.	15
Figure 18. Comparison of the Charpy impact energies of the as-received material to that of the material aged at 650°C for various times. Note that the test temperature only indicates the temperature at which the test was performed, not the aging temperature.....	16
Figure 19. Plots comparing the crack growth rates vs. frequency for the as-received material and four aging times at 650°C. The data in each plot was generated under fatigue crack growth conditions at constant maximum stress intensity (K_{max}).	18
Figure 20. Crack length vs. time for compact tension specimens tested under quasi static loading conditions at $K = 40 \text{ MPa}\sqrt{\text{m}}$	19
Figure 21. Bright field TEM micrograph showing interaction of γ' particles with mobile dislocations during creep at 750°C and 145 MPa, ~10% strain, 2127 hrs.....	20
Figure 22. Schematic drawing showing the "shoulder" areas where TEM samples were taken γ' particle size analysis.	20
Figure 23. Dark field image (left) and the associated diffraction pattern (right) of I-617 statically aged at 750°C for 650 hrs.	21
Figure 24. Gamma prime particle size distribution as a function of static aging time at 750°C.....	22
Figure 25. Plot of the average particle radius as a function of aging time.....	22
Figure 26. Plot of the cube of the average particle radius as a function of aging time.	23
Figure 27. Plot of the γ' growth constant, k , versus reciprocal temperature. The grow rate constant for the data obtain from the 750°C creep tests yields a temperature in the shoulder region of the creep specimen of approximately 738°C.....	25
Figure 28. Zener-Hollaman type plot for creep of Alloy 617.....	26
Figure 29. Linear plot of strain rate to the 1/m power plotted against stress, from which the threshold stress can be determined.	27

Figure 30. Zener-Hollaman type plot for Alloy 617 creep data with a threshold stress of 65 MPa applied to the data for 750°C.....	27
-----------------------------------------------------------------------------------------------------------------------------------	----

TABLES

Table 1. Summary of testing done on Alloy 617 to support previous reactor programs.	2
Table 2. Chemical composition (wt. %) of Alloy 617.	3
Table 3. Fracture properties of solution annealed Alloy 617.....	7
Table 4. Summary of the tensile properties of Alloy 617 which has been aged for various times at 650°C. The as-received tensile properties are also shown for comparison.	14
Table 5. Growth Rate Constants.	23
Table 6. Estimated γ' Particle Radius after 100,000 hours.	25

ACRONYMS

ASME	American Society of Mechanical Engineers
ASTM	American Society for Testing and Materials
B&PV	Boiler and Pressure Vessel
CMS	controlled material specification
CVN	Charpy V-notch
DOE	Department of Energy
FY	fiscal year
GIF	Generation IV International Forum
GT MHR	Gas Turbine Modular Helium Reactor
HTGR	high temperature gas cooled reactor
HTR	High Temperature Reactor
HTTR	High Temperature Engineering Test Reactor
IHX	intermediate heat exchanger
INL	Idaho National Laboratory (formerly the Idaho National Engineering and Environmental Laboratory)
MHTGR	modular high-temperature gas-cooled reactor
NGNP	Next Generation Nuclear Plant
NRC	Nuclear Regulatory Commission
ORNL	Oak Ridge National Laboratory
PCHE	printed circuit heat exchangers
PCS	power conversion system
PCU	power conversion unit
PFHE	plate fin heat exchanger
PHTS	primary heat transport system
PHX	process heat exchanger
R&D	research and development
SG	steam generator
SG-ETD	Subgroup on Elevated Temperature Design
SHTS	secondary heat transport system
SSC	safety significant components
TEM	transmission electron microscopy
VHTR	very high-temperature reactor

Aging of Alloy 617 at 650 and 750°C

INTRODUCTION

Input from potential end-users indicates that process applications, especially for future (nth of a kind) VHTR deployments, will require delivery of high temperature heat through heat exchangers. Presumably future VHTRs based on the NGNP design will operate at higher temperatures; temperatures as high as 1000°C have been targeted. The IHX is likely the component most critically impacted by increased temperatures. The outlet gas temperature does not affect material selection for the IHX in the range of 750-900°C; however, it may affect the design allowable stresses.

The IHX transfers thermal energy between the primary and secondary heat transport system (PHTS – SHTS). The PHTS includes the primary circulator, primary piping, and primary helium working fluid. The SHTS has secondary piping and a secondary working fluid (such as He or a He-N₂ mixture) that will transport heat to downstream applications such as H₂ production, process heat, and power production (i.e., steam production). The IHX also separates the primary and secondary power generation circuits and would separate a hydrogen generation plant from the major reactor systems. This will minimize the potential for tritium migration, and ensure accident or upset conditions in a hydrogen production facility do not impact the operation of the reactor. Components of the IHX are the heat exchanger cores and/or modules containing the heat transfer surfaces, the IHX vessel, and the headers and/or piping. Although the inlet temperature for the IHX would be quite high, the outlet temperature would be in a range where reduced properties resulting from aging will be a concern.

A number of solid solution strengthened nickel- and iron-based alloys have been considered for application in the VHTR program. The primary candidates were Alloy 617, Alloy 230, Alloy 800H and Alloy X. Based on the technical maturity, availability in required product forms, experience base, and high temperature mechanical properties, all of the pre-conceptual design studies prepared by potential reactor vendors have specified Alloy 617 as the material of choice for heat exchangers. Also a draft ASME Code case for Alloy 617 was developed previously. Although action was suspended before the Draft Alloy 617 Code Case was accepted by ASME, it provides a significant basis for achieving codification of the material. Alloy 800H qualification for use up to 850°C is currently in the approval process for use in nuclear design. This alloy is the preferred candidate for a VHTR with an outlet temperature in the range 700 to 750°C employing a steam generator rather than an IHX. The allowable stresses for Alloy 800H may not be sufficient at these temperatures for the steam generator and Alloy 617 may be required for this component because of its higher strength.

BACKGROUND

Alloy 617, also designated as Inconel 617, UNS N06617, or W. Nr. 2.4663a, was initially developed for high temperature applications above 800°C. It is often considered for use in aircraft and land-based gas turbines, chemical manufacturing components, metallurgical processing facilities, and power generation structures. The alloy was also considered and investigated for the HTGR programs in the United States and Germany in the late 1970s and early 1980s. Alloy 617 is not currently qualified for use in ASME Boiler and Pressure Vessel (B&PV) Code Section III, although it is allowed in Section I and Section VIII, Division 1 (for non-nuclear service). A draft ASME Code case for incorporating Alloy 617 in Section III was developed but efforts to gain the approval from the ASME Code committees were suspended prior to final approval.

This nickel-based alloy is the primary candidate for construction of a VHTR IHX, and the existing mechanical property database is extensive (Table 1),¹ some of which was used to develop existing ASME B&PV Code, and the 1980s Draft Alloy 617 Code Case mentioned above. In addition, some studies have generated data from Alloy 617 that had been aged and/or tested in simulated HTGR helium, with more recent efforts preserving all original test curves needed for constitutive modeling efforts. A summary of previous work is given in Table 1.

Alloy 617 retains some creep strength at temperatures above 870°C, the alloy has good cyclic oxidation and carburization resistance, and good weldability. It also has lower thermal expansion than most austenitic stainless steels and high thermal conductivity relative to the other candidates. It retains toughness after long-time exposure at elevated temperatures and does not form complex intermetallic phases that can cause embrittlement.

Table 1. Summary of testing done on Alloy 617 to support previous reactor programs.

Research Organization	Number of heats	Number of samples	Test type	Temperature (°C)
Huntington Alloys	13 + 1wire	179	Tensile	25-1093
		249	Creep	593-1093
ORNL ^a	4 plate + 1 wire	73	Tensile	24-871
		51	Creep	593-871
		25	Charpy	24
		1	Tensile after creep	RT after 871
GE ^a	1 plate + 1 bar	36	Creep	750-1100
		7	Creep-fatigue	950
		40	Fatigue	850, 950
Germany	Not specified	302	Tensile	RT-1000
		1947	Creep	500-1000
		29	Creep crack growth	700-1000
		261	Low cycle fatigue	<500-1000
Honeywell Aerospace	Not specified		Not specified	
Gen IV program ^b	Not specified	80	Creep-fatigue	800, 1000

a. some tests exposed to HTGR environment.

b. air, pure helium and vacuum environments.

Two 1.397 m × 3.505 m (55 in. × 138 in.) of 38 mm (1.5 in.) thick plates of solution annealed Alloy 617 from a single heat (cast 314626) were procured from ThyssenKrupp VDM for the NGNP R&D program. This heat of material serves as the reference material for the majority of the NGNP related R&D. All mechanical test specimens for which results are discussed below were machined from annealed plate; the long axis of the specimen aligned with the rolling direction.

The ASTM specified chemical composition of Alloy 617 and that of the procured heat are given in Table 2.² The high Ni and Cr contents provide the alloy with high resistance to a variety of reducing and oxidizing environments. The Al, in conjunction with Cr, offers oxidation resistance at high temperatures. In addition, the Al and Ti can also form the intermetallic compound γ' over a range of temperatures, which results in precipitation strengthening in addition to the solid solution strengthening imparted by the Co and Mo. Strengthening is also derived from $M_{23}C_6$, M_6C , Ti(C, N) and other precipitates when in appropriate sizes, distributions, and volume fractions. A time-temperature-transformation (TTT) diagram for this alloy is shown in Figure 1.

Solution annealed Alloy 617 in the as-received condition is very ductile. Because of its high fracture toughness, J-R Curve testing for Alloy 617 is very difficult to conduct; hence, not many fracture toughness data are reported in the literature. Figure 2 shows a J-R Curve at 700°C, and Figure 3 (a) and (b) show the values of J_0 (onset of stable ductile tearing) and the tearing modulus, respectively, as a function of test temperatures from the literature.⁴ The multi-specimen technique was used in determining the J-R Curve.^{5,6}

As observed from Figure 3(a), a small increase occurs in J_0 between 35 and 200°C, and it remains constant from 200 to 725°C, then a strong increase occurs at 750°C. Krompholz et al.⁴ reported that no onset of stable tearing was detectable up to a J-integral value of 2500 kJ/m² at temperatures of 775°C and above.

Table 2. Chemical composition (wt. %) of Alloy 617.

	Ni	Cr	Co	Mo	Fe	Mn	Al	C	Cu	Si	S	Ti	B
Min	44.5	20.0	10.0	8.0	—	—	0.8	0.05	—	—	—	—	—
Max	—	24.0	15.0	10.0	3.0	1.0	1.5	0.15	0.5	1.0	0.015	0.6	0.006
TK31426	54.1	22.2	11.6	8.6	1.6	0.1	1.1	0.05	0.04	0.1	<0.002	0.4	<0.001

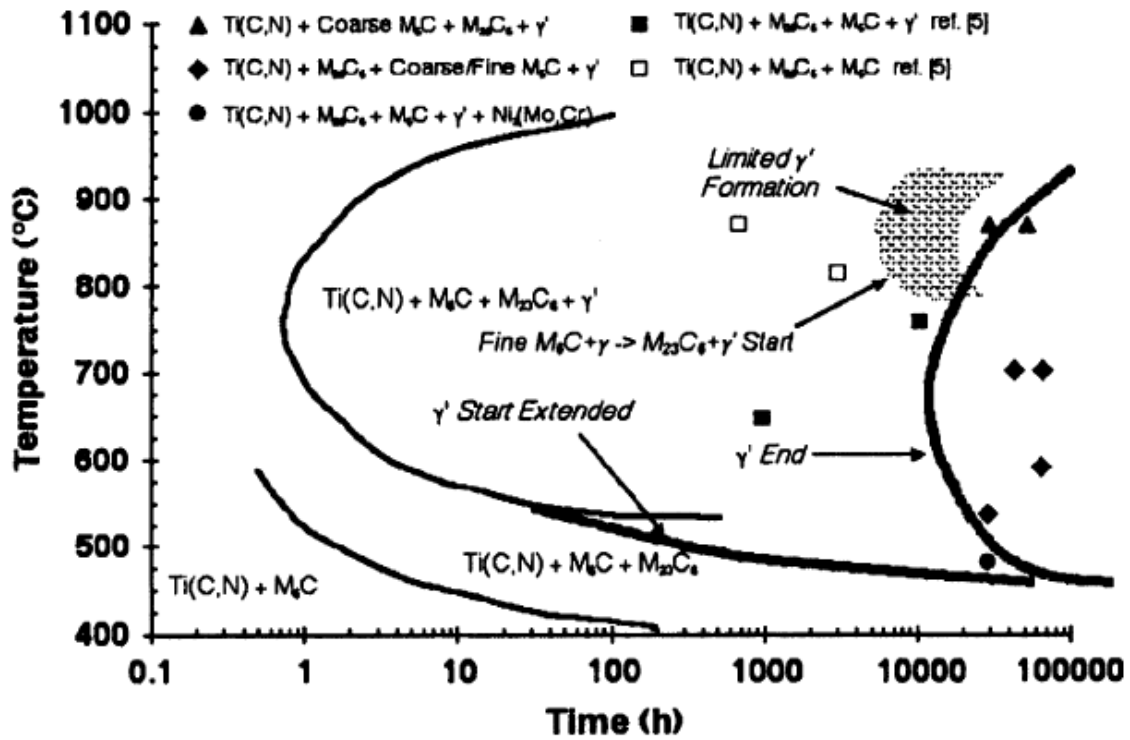


Figure 1. Time-temperature-transformation (TTT) diagram for long term aging of Alloy 617.³

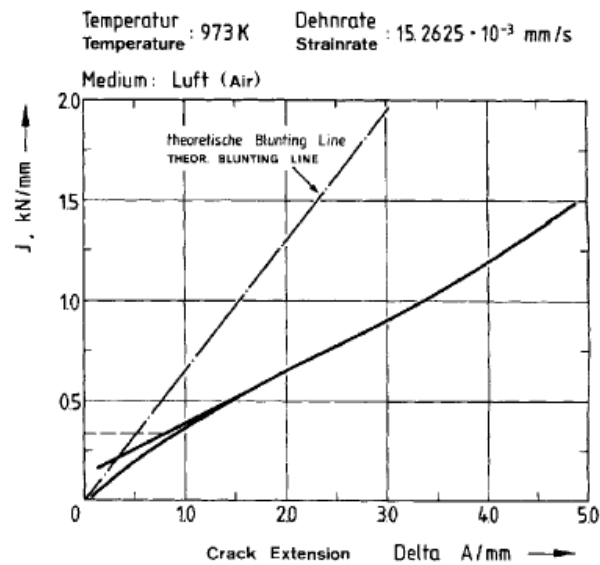


Figure 2. J-R Curve for solution annealed Alloy 617 at 700°C.

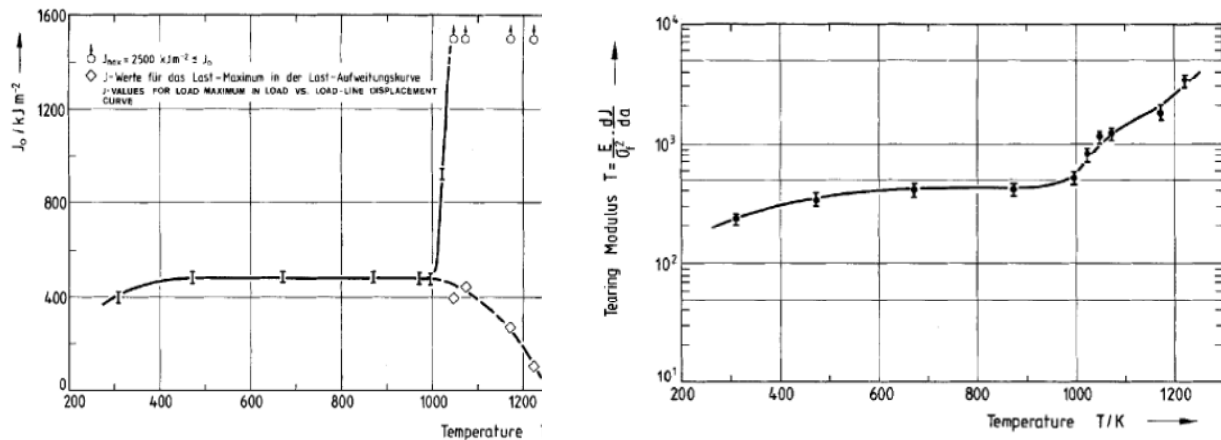


Figure 3. (a) Values of J_0 and (b) tearing modulus for Alloy 617, as received (temperature in Kelvin).

No J-R Curve or toughness data were found from the literature on thermally aged Alloy 617. However, data on room-temperature Charpy V-Notch (CVN) energies from thermally aged Alloy 617 have been reported⁷ and are shown in Figure 4. It is seen that the room-temperature CVN energy dropped significantly, depending on the thermal exposure temperature and time, from an averaged unaged value of 170 ft-lb, to as low as 30 ft-lb for aged Alloy 617. Figure 5 shows the CVN energy for aged Alloy 617 measured at room temperature and aging temperature.⁸ The room-temperature CVN energy dropped to below 10 J after exposure at 800 and 900°C for 10,000 h.

ASME codification requires a fracture mechanics analysis to justify the ability of Alloy 617 to withstand the expected service conditions, especially when the component cools down to lower temperatures after extended exposure at elevated temperature. Tests of 0.5T compact tension specimens from solution annealed Alloy 617 plate from the NGNP heat have been performed at room temperature, 100, 250, 750, and 850°C as part of the previous work carried out in the NGNP program. Some of those results will be summarized here. All specimens were fatigue pre-cracked to a crack length/width ratio of about 0.5. The maximum load during the test, the provisional value of J-integral at onset of crack initiation (J_q), and the tearing modulus are tabulated in Table 3. For the tests at 750 and 850°C, values of J_q and tearing modulus could not be calculated because crack extension did not occur in the specimens under these loading conditions. The rows printed in bold font in the table are the average values of multiple tests at the indicated temperature.

At room temperature, the ductile initiation fracture toughness, J_q , for this unaged Alloy 617 material is about 800 to 900 kJ/m^2 and the tearing modulus (dimensionless) is about 130. These values are reflective of a very tough material. The results at test temperatures of 100 and 250°C were very similar in behavior and in toughness values to those at room temperature. The load versus crack-mouth opening displacement record and a plot of J versus Δa (crack extension) for one of the fracture toughness tests performed at room temperature are shown in Figure 6.

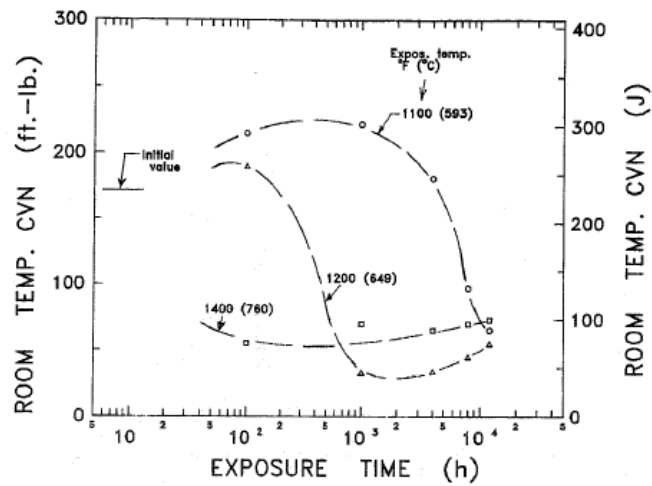


Figure 4. Room temperature CVN energy of Alloy 617 after thermal exposure.

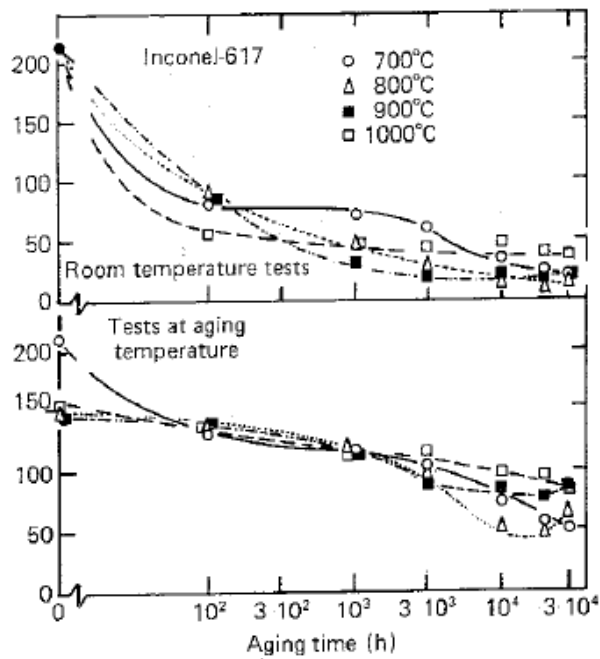


Figure 5. CVN energy of aged Alloy 617 measured at room temperature and aging temperature.

Table 3. Fracture properties of solution annealed Alloy 617.

Test Temperature (°C)	Maximum Load (lbs)	Jq (psi) (kJ/m ²)		Tearing Modulus
RT	2900	5167	904	126
RT	3050	4844	848	131
RT	3200	4520	791	135
100	2750	4046	708	96
100	2775	4275	748	107
100	2800	4504	788	117
250	2800	5165	904	139
250	2900	4722	826	146
250	3000	4278	749	153
750	2600	No CG	No CG	No CG
850	1300	No CG	No CG	No CG

RT ≡ Room Temperature
CG ≡ Crack Growth

In addition to the NGNP fracture mechanics testing, eighteen Charpy V-notch (CVN) impact specimens of solution annealed (unaged) Alloy 617 have been tested. Half of these were aligned with the rolling direction, and half transverse to the rolling direction. The results indicate no significant effect of notch orientation for this heat of Alloy 617. CVN impact specimens, from Alloy 617 aged for 200 hours at 750, 800, 850, 900, 950, and 1000°C, have also been tested. Figure 7 shows the CVN results obtained for the solution annealed (unaged) specimens and specimens aged at 950°C. Figure 8 provides a graphical summary of the test results for all the CVN tests. The diamond symbols represent the absorbed energy measured at room temperature for each case. The square symbols represent a test temperature of 250°C, the test temperature with the highest absorbed energy measured over the range of test temperatures (up to 950°C) for each aging condition.

The greatest change in Charpy energy was seen after aging at 750°C. This is consistent with the TTT diagram shown in Figure 1 where it can be seen that the most rapid formation of precipitates occurs at this temperature. Subsequent to these preliminary experiments it became apparent that long time aging at this temperature and below had the greatest potential for affecting properties. As a result, the effect of a more extensive series of aging times at 650 and 750°C on microstructure and properties was determined. Results of those studies for aging times up to 5,300 hours are discussed below.

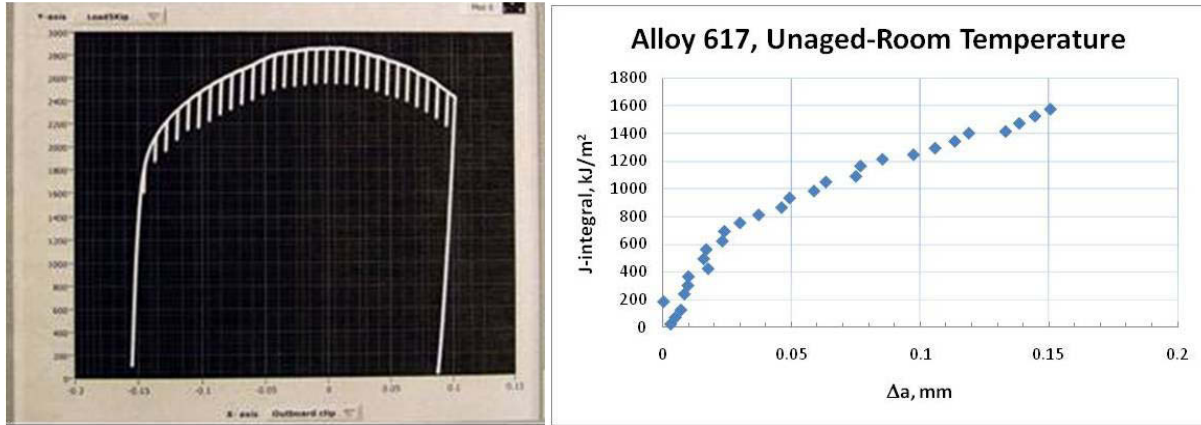


Figure 6. Load vs. crack mouth opening displacement record and a plot of J versus Δa (crack extension) for a 0.5T compact fracture toughness test performed at room temperature.

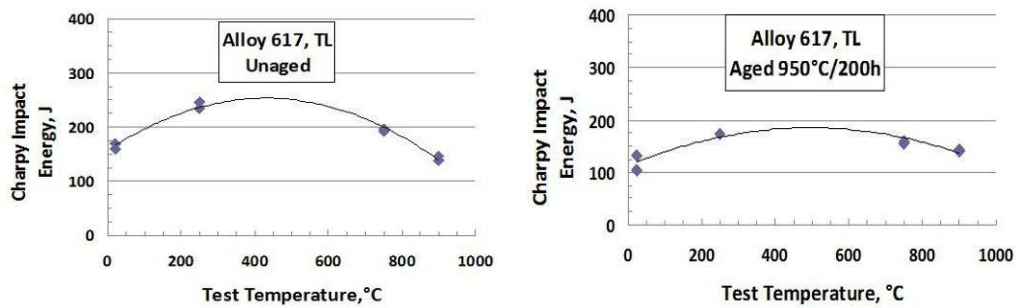


Figure 7. Charpy impact energies for solution annealed and aged Alloy 617 tested at temperatures from ambient to 900°C.

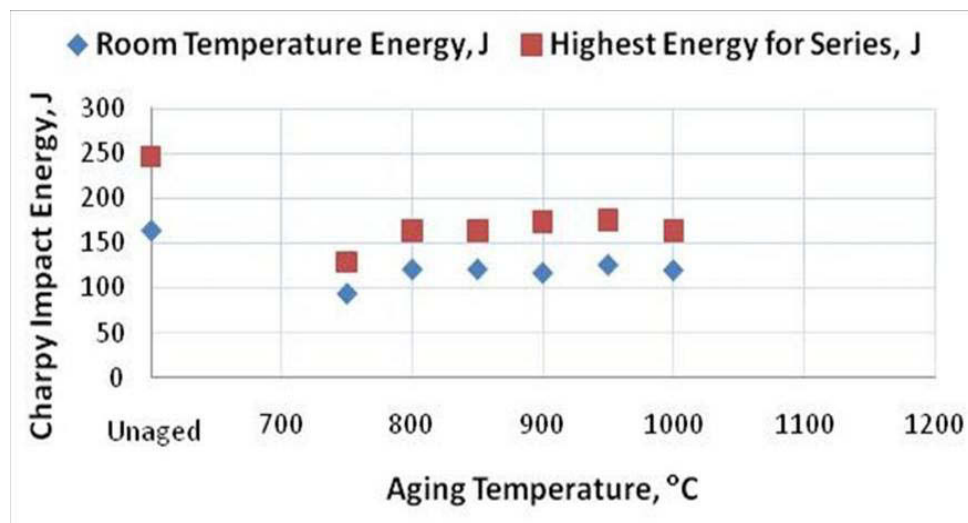


Figure 8. Highest observed CVN impact energies of solution annealed and aged Alloy 617.

RESULTS AND DISCUSSION

Optical Microstructure

The microstructure for optical microscopy on the as-received and aged Alloy 617 material was revealed using an electrolytic etching technique. Samples were prepared first by grinding to 800 grit SiC paper and then electrolytically polishing and etching using a Streurs ElectroPol-5 and a perchloric acid electrolyte solution. The etching voltage and times had to be adjusted between the as-received and aged material since the etching behavior was very different. This difference in etching behavior is indicative of chemistry changes in the aged matrix material versus the solution annealed alloy.

As-Received Microstructure

The as-received microstructure is characterized by carbide banding and stringers which can be seen in Figure 9. In the areas of the matrix outside these banded regions, there are few to no secondary particles besides a small number of titanium nitrides (TiN). The bands range from approximately 100-300 μm wide. Within the carbide bands/stringers, the carbides appear to form a cell structure which is independent of the present grain boundary structure (i.e. cell boundaries traverse the current boundaries without any interaction). It is possibly that this carbide cell structure relates to the previous GBs from the hot-rolling before the anneal process. Then, after the matrix had recrystallized during cooling from the anneal process, the carbides may have stayed in the former grain boundary position and/or precipitated on the boundaries or residual dislocation from this previous structure.

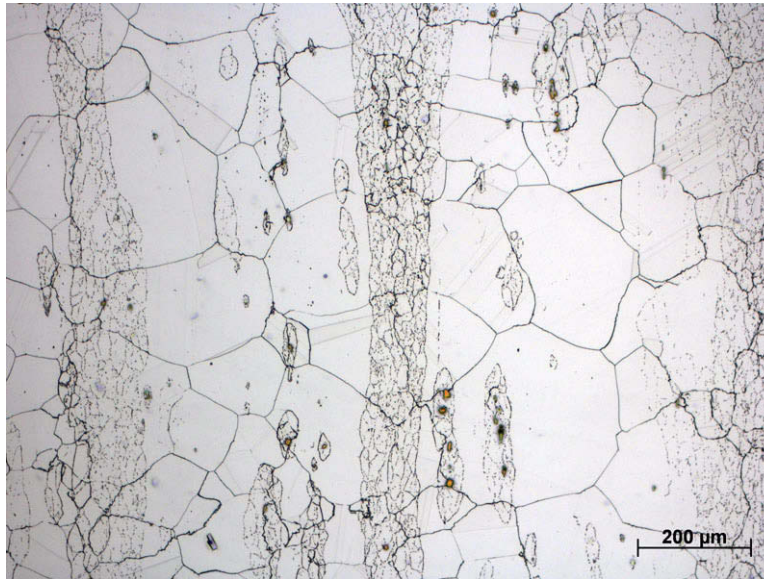


Figure 9. Optical microstructure of the as-received Alloy 617 material at 100x magnification and oriented with the rolling direction in the y-axis. The as-received material shows significant banding which is apparent in the image.

Microstructure After Aging 200 Hours

The Alloy 617 plate shows an evolution of microstructure even after aging for relatively short period of 200 hours at both 650 and 750°C. This observation is consistent with the TTT diagram for Alloy 617 which shows that M_{23}C_6 , M_6C , and γ' will start precipitating in as little as one hour at these temperatures.³ Comparing the as-received microstructure to that of aged material, both the 650 and 750°C show a similar amount of carbide precipitation after 200 hours as seen in Figure 10 and Figure 11. There is still some banding present in both 200 hour aging microstructures, but the new carbide precipitation has slightly obscured the previous areas with banding or stringers.

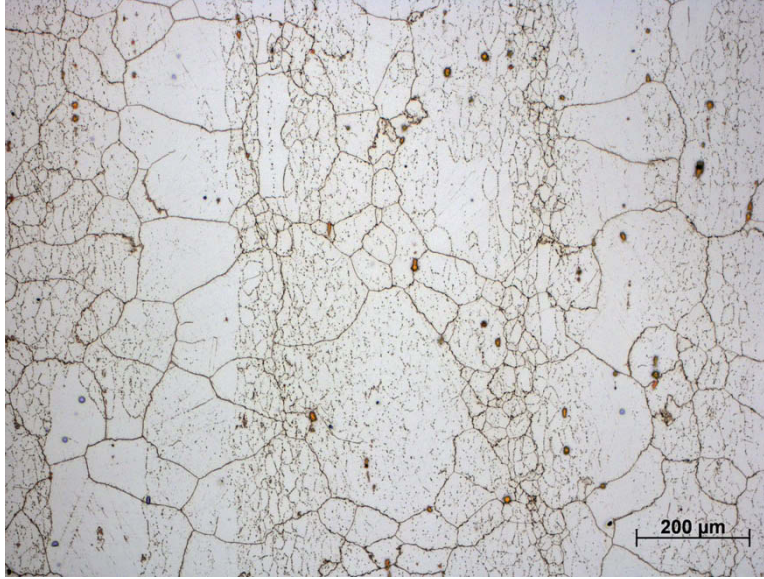


Figure 10. Image showing the optical microstructure of plate aged at 650°C for 200 hours. The orientation and magnification are the same as in Figure 9.

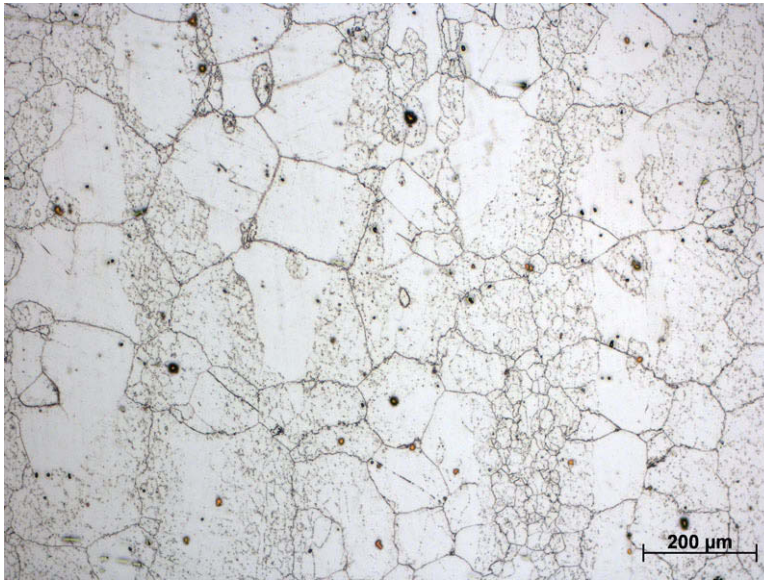


Figure 11. Microstructure of the plate aged at 750°C for 200 hours. The orientation and magnification are the same as in Figure 9.

At both aging temperatures, the majority of carbides are intragranular and there is no indication of carbide redistribution or precipitation directly on the grain boundaries. The carbides appear to partly retain the cell structure seen in the as-received material in the banding regions. However, the material aged at 750°C does show a difference in the regions adjacent to the carbide bands. In the grains without large dispersions of carbides (i.e. mainly carbide free grains), higher magnification optical micrographs indicate that carbides have precipitated adjacent to GBs as seen in detail (b) of Figure 12. The plate aged at 650°C for 200 hours does not show this behavior. Furthermore, dense precipitation of very fine carbides is visible around TiN particles after aging at 750°C which can also be seen in detail (b). The

thermal mismatch between the nitrides and gamma matrix may have generated a higher density of dislocations as the alloy was cooled from the annealing temperature which would then serve as nucleation sites for carbides during subsequent high temperature exposure. In contrast, the as-received Alloy 617 and material aged at 650°C only show discrete “rings” of coarse carbides round TiN precipitates which likely formed during the solution anneal. The discrete rings are no longer apparent around the nitrides after aging at 750°C. In both the as-received material and both aging temperatures, there are still some nitrides which show no indication of carbide precipitation.

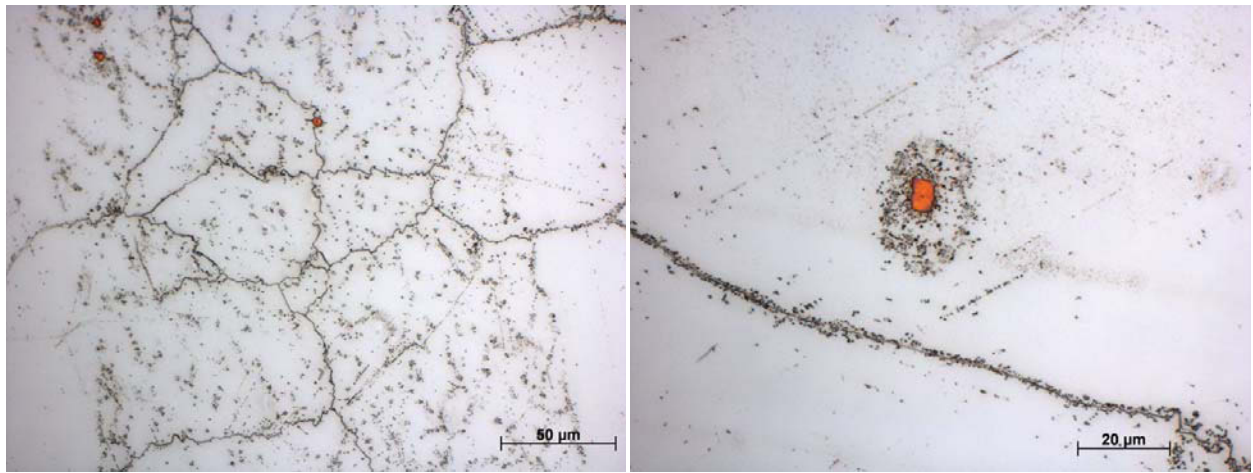
Another difference between the as-received and aged material is the nature of the grain boundaries within the banded regions. Detail (a) in Figure 12 shows the serrated morphology of the grain boundaries which can be seen in the carbide band regions at both aging temperatures. The as-received material does have some serrated boundaries in similar areas, but the degree of serration is much smaller. These serrations in the aged material indicate that there are small amounts of grain movement and coarsening during high temperature exposure. One likely explanation for the serrations in the grain boundaries is that secondary phases such as grain boundary carbides pin sections of the grain boundary during migration, thus causing the irregular boundary. Another contributor may be related to the diffusion of carbon along the grain boundaries. Comparing Figure 12a (within region of carbide band) to Figure 12b (non-banded region) in the material aged for 200 hours at 750°C, carbon appears to be diffusing from the banded regions to the non-banded regions. There is no indication of new carbide precipitation adjacent to boundaries in the banded regions. Since carbon could be using the grain boundary as a fast diffusion path, a flux of vacancies in the opposite direction would be necessary. Any flux divergence between the vacancies and carbon atoms in the banded regions would cause vacancies to pile up on the grain boundary, thus allowing for climb of the grain boundary dislocations and small serrations to form.

Microstructure After Aging 5300 Hours

The microstructure of the plate aged for 5300 hours at 650°C does not show a large evolution compared to that of the plate aged for 200 hours. As seen in Figure 13, slightly more carbide precipitation occurred in the regions previously free from carbides after 5300 hours. There are not any more significant differences in the microstructures for these two aging times. The 5300 hour microstructure still shows the carbide cell structure in the banded regions as before.

The difference in microstructure between 200 and 5300 hours at 750°C is much more significant. A micrograph of the plate after 5300 hours is shown in Figure 14. The carbide banding has become increasingly difficult to distinguish due to large amounts of carbide precipitation. Furthermore, the cell structure within the banded regions is masked by the new carbide precipitation. However, a few discrete strips largely free from carbides still remain between bands. In these strips, some carbides have precipitated on slip lines in the middle of the grains.

Another distinguishable feature of the microstructure after aging for 5300 hours at 750°C is that carbides have clumped together into small groups. This is shown clearly in Figure 15. The authors of a previous aging and mechanical study on Alloy 617 called these “sunburst” patterns and they were found in creep samples tested at 816°C and 69 MPa for approximately 3000 hours.⁹ In this work, the morphology of these clusters consisted of a center polyhedral particle with many small carbides which had precipitated around its periphery. The authors of this paper were not able to do any quantitative TEM analysis on the center particles of these groups since the particles would either drop through TEM foils during preparation or sample were too thick to perform TEM analysis. Other work indicated that the center particles were very similar to the shapes of isolated $M_{23}C_6$ carbides. Similar to the fine precipitation around the TiN particles at shorter times, carbide growth during the annealing process likely created dislocations which provided nucleation sites for new precipitation during subsequent aging.



(a)

(b)

Figure 12. Two images of the microstructure from plate aged at 750°C for 200 hours. (a) shows the serrated nature of the grain boundaries caused by grain movement in a small region of the plate and (b) shows the migration of carbides to regions directly adjacent

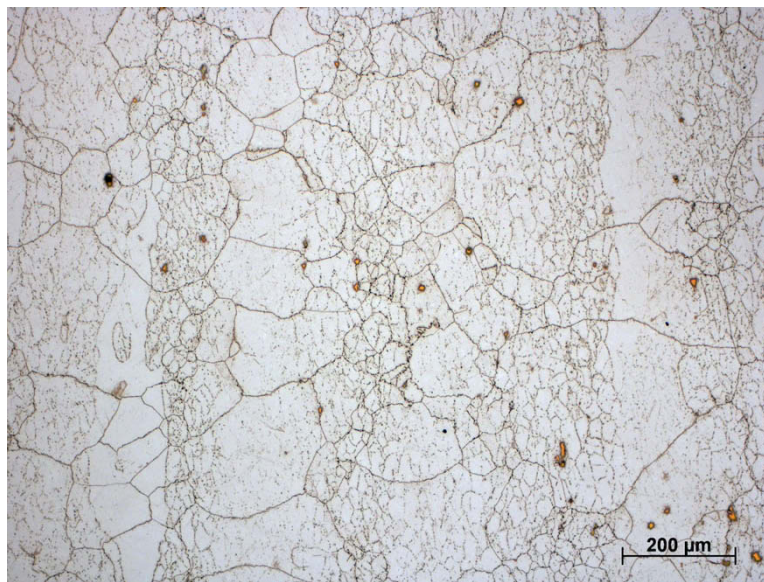


Figure 13. Microstructure of the plate after aging for 5300 hours at 650°C. The orientation and magnification are the same as in Figure 9.

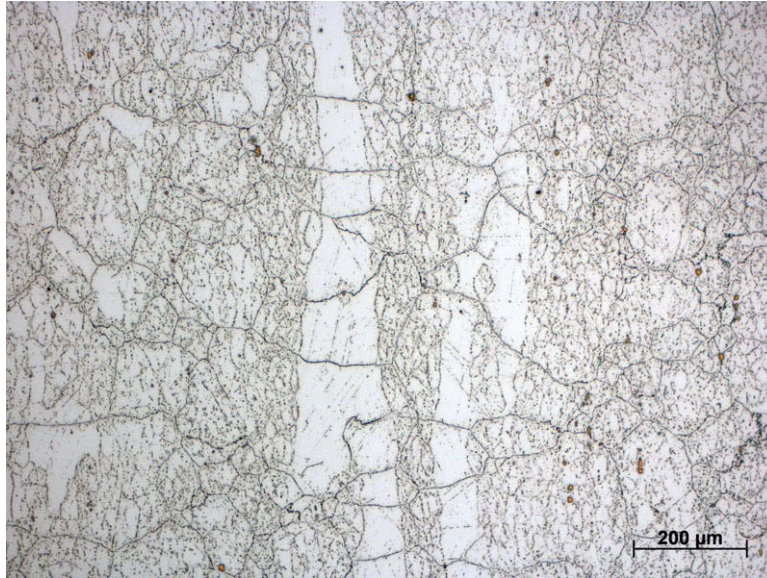


Figure 14. Optical microstructure of the plate after aging at 750°C for 5300 hours. The orientation and magnification are the same as in Figure 9.

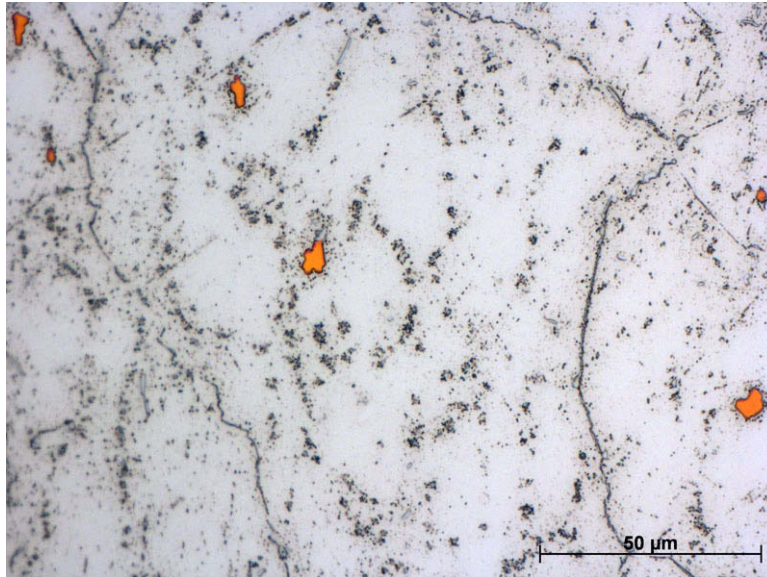


Figure 15. High magnification optical micrograph of the material aged at 750°C for 5300 hours. Clusters or sunburst patterns of carbides are apparent in this image.

Mechanical Testing on Aged Material

Tensile Results

The tensile data for Alloy 617 aged at 650°C were obtained using an electromechanical type Instron test machine. The crosshead speed was kept constant through the entire test at approximately 1.25 mm/min which achieves a strain rate of approximately $3.6 \times 10^{-2} \text{ s}^{-1}$. The specimen strain was measured directly in the 0-20% range using an extensometer and then estimated from 20% until fracture using the crosshead displacement.

Table 4 summarizes the tensile test results of the aged plate. The strength and ductility properties of the as-received solution annealed plate are included for comparison. Furthermore, the aged material was tested both at room temperature and 650°C. Comparing the room temperature as-received tensile results to that of the aged plate, it is clear that the tensile strength of the plate increases as aging time increases at 650°C. This strengthening is expected due to the precipitation of γ' which provides additional dislocation pinning. New carbide precipitation may also provide a small amount of strengthening over the as-received material. Figure 16 compares the as-received tensile curve to the curves of the four 650°C aging times at room temperature. As the aging time is increased, the tensile curves indicate that the work hardening rate is also increases as expected due to the increase in density of secondary phases. Furthermore, a corresponding decrease in ductility is observed as the aging time is increased.

The tensile results for the aged Alloy 617 at a test temperature of 650°C are shown in Figure 17. Again, the yield and tensile strengths of the aged material show very similar increases between the aging times as the room temperature results. The difference between the room temperature and 650°C tests is that the 650°C tensile curves indicate the material begins to soften at the longer aging times whereas the room temperature tensile tests do not show this behavior. None of the tensile specimens indicate any significant amount of necking. Also, the ductility values from the 650°C do not show any consistent trend between the aging times, in contrast to the room temperature tests. Softening of the material before fracture could explain this.

Table 4. Summary of the tensile properties of Alloy 617 which has been aged for various times at 650°C. The as-received tensile properties are also shown for comparison.

Aging Time (h)	Test Temperature (°C)	Yield Stress (MPa)	Tensile Strength (MPa)	Ductility (%)
as-received	25	314	768	62
200	25	449	910	51.5
650	25	487	930	46.2
2000	25	512	974	43
5300	25	532	982	42.1
200	650	347	668	53.3
650	650	384	721	51
2000	650	414	751	54.1
5300	650	435	766	56.7

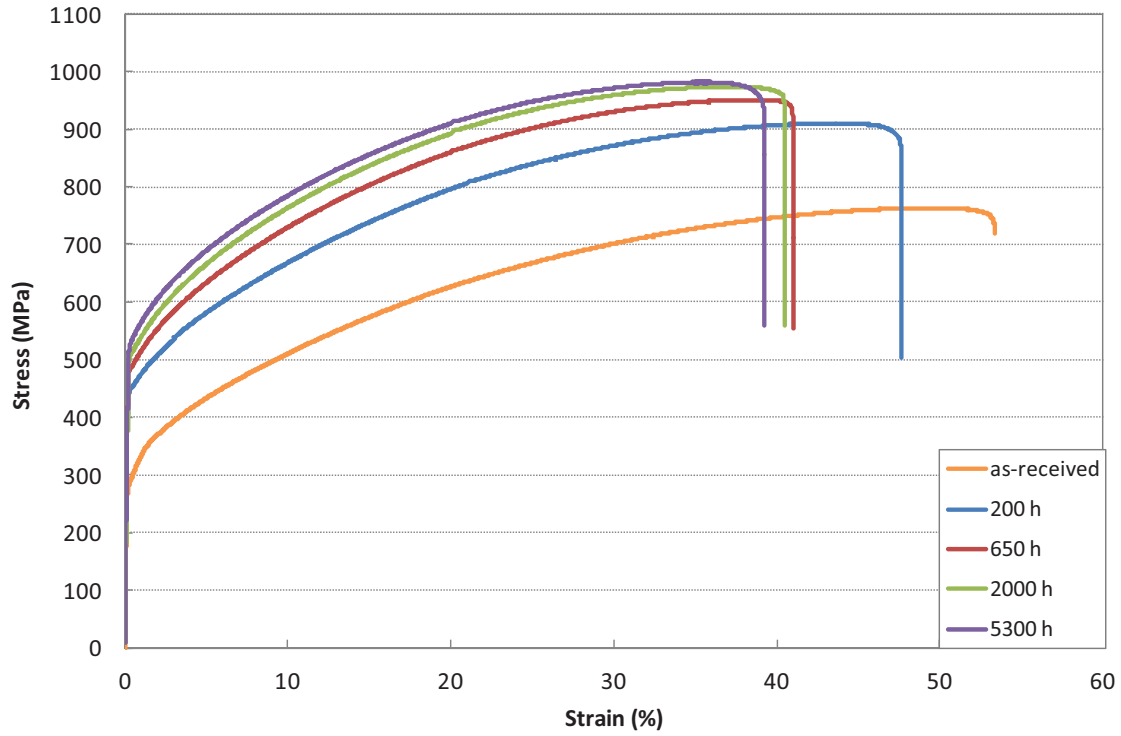


Figure 16. Room temperature tensile test results of the as-received material and material aged at 650°C for various times.

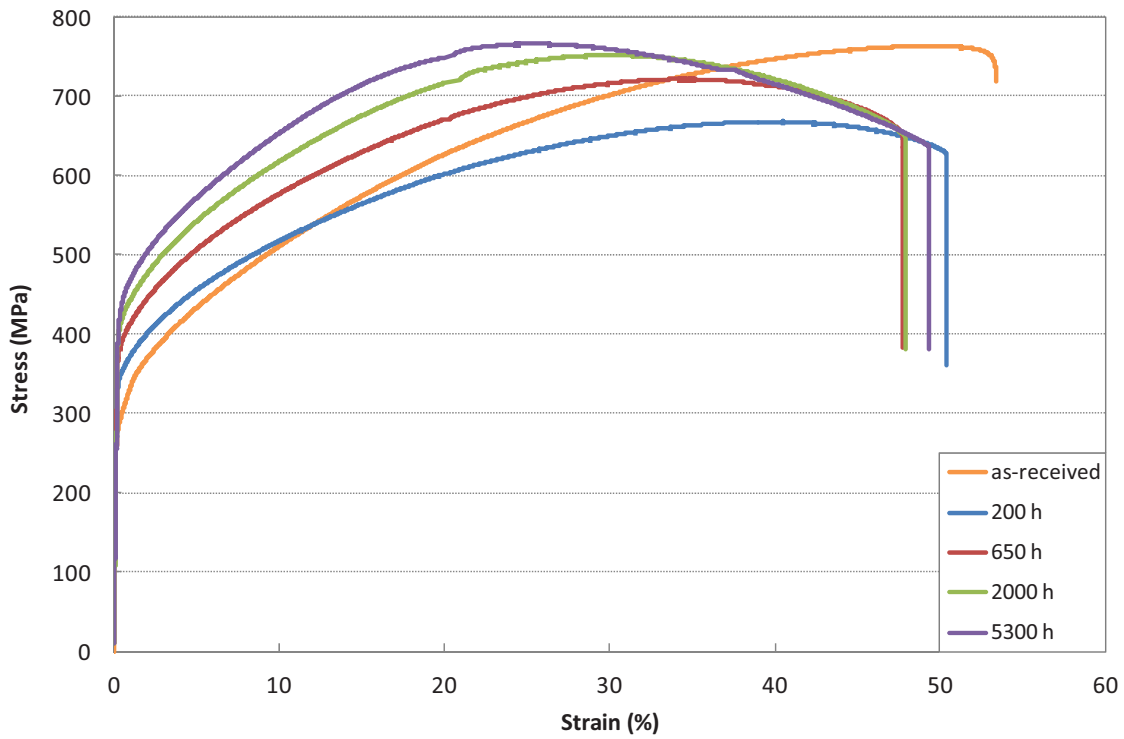


Figure 17. Tensile test results for material aged at 650°C for various times and a test temperature of 650°C. The as-received material tensile results for comparison are at room temperature.

Charpy Impact Energy

Impact tests were conducted on both the as-received and material aged for various times at 650°C. Data were obtained at room temperature and five higher temperatures: 250, 550, 650, 750 and 850°C. These test temperatures were chosen to bracket any behavior in the 650-750°C aging temperature range. Furthermore, two orientations were tested on the as-received and each aging condition: one orientation with the fracture propagating parallel to the rolling direction (T-L) and one orientation with the fracture propagating perpendicular to the rolling direction (L-T). The results from these tests are summarized in Figure 18. Since the impact energies did not display any orientation dependence, the average energies are plotted for each aging time/test temperature.

The as-received Alloy 617 has impact energies above 150 J for all of the test temperatures. Figure 18 indicates the energies increase from room temperature, reach a maximum between approximately 450 and 550°C, and then decrease as the temperature increases beyond this range. Comparing the material aged at 650°C to the as-received material, the Charpy impact energies drop more than 50% at room temperature for all of the aging times. As the test temperature is increased, a general increasing trend in the impact energies is observed for all of the aging times and the highest energies for the aged material are seen at 850°C. The difference in energies between the as-received and aged material decreases as the test temperature is increased until almost no difference is observable at 850°C. Furthermore, comparing the impact energies of the various aging times, it is observed that an increase in the aging time decreases the energy, with the largest energy differences in the range of 550-750°C. Lastly, it should be noted that small inconsistency in the energies exists at 650°C for the aged material. Figure 18 shows a small decrease in the energy at 650°C from 550°C, and then the energies increase again after 650°C. Other Alloy 617 material properties such as electrical and thermal conductivity show a similar dip in magnitude in this temperature range and has been discussed elsewhere.¹⁰ The short range ordering which occurs at this temperature and gives rise to the inconsistencies in conductivity and other properties may be related.

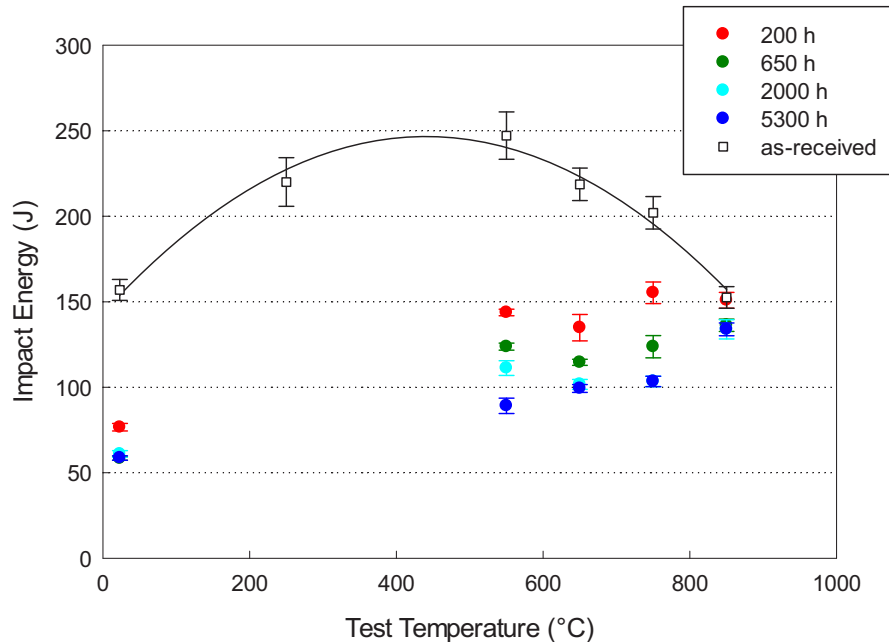


Figure 18. Comparison of the Charpy impact energies of the as-received material to that of the material aged at 650°C for various times. Note that the test temperature only indicates the temperature at which the test was performed, not the aging temperature.

Crack Growth

Crack growth rates for Alloy 617 aged at 650°C were acquired and compared to the growth rates in the as-received material. These data were obtained under various constant maximum stress intensities (K_{\max}) and fatigue and creep-fatigue conditions. The fatigue crack growth was conducted using a triangular waveform at 0.5, 0.1, 0.05, and 0.01 Hz and a trapezoidal waveform for creep-fatigue. For the trapezoidal loading, various hold times at maximum load were selected: 10, 60 and 300 s.

The fatigue and creep-fatigue crack growth rates for the aged material are shown in Figure 19. The as-received crack growth rates are also included in each plot for comparison purposes. Both the as-received and aged material show an increase in the crack growth rate in mm/cycle as the frequency is decreased. Aging time at 650°C does not indicate any impact on this trend. The increase in crack growth rate with a decrease in frequency is likely due to environmental interactions with the crack tip but is not the focus of this discussion. The $K_{\max} = 30 \text{ MPa}\sqrt{\text{m}}$ does indicate that differences in the crack growth rates between the several aging times may arise as the higher stress intensities under fatigue and creep-fatigue loading. Only the specimens aged for 5300 hours show a small decrease in the crack growth rates at this higher stress intensity. However, the error bars on the mean crack growth rate for the as-received material general envelope all of the rates for the aged material, which makes any conclusions difficult to make without more testing and analysis.

Changes in the crack growth rates with aging time were not expected under fatigue loading. Within a given material system, the crack growth per cycle is generally not sensitive to microstructure and monotonic flow properties. Rather, fatigue crack propagation is thought to be controlled by cyclic flow properties, not monotonic flow properties. Although Alloy 617 exhibits considerable increases in its tensile strength at 650°C, the cyclic stress-strain curve would trend towards those of the as-received material, which is relatively insensitive to the initial strength levels. However, it is surprising that the creep-fatigue crack growth rates do not show more difference between the as-received and aged material. More investigation is needed to explain this negligible difference under creep-fatigue crack growth conditions.

Crack growth studies under quasi-static loading (i.e. creep) conditions were also completed at 650°C and a stress intensity of $K = 40 \text{ MPa}\sqrt{\text{m}}$. These results are shown in Figure 20. This plot does show an environmental effect on the creep crack growth in which the impure helium environment increases the crack growth rate compared to the air environment. However, this environmental effect will not be discussed in further detail as material aging is the focus of this study. In Figure 20, the crack growth rate increases with time which may be due to aging of the material. Since the fracture is primarily intergranular under these conditions, aging of the material could potential change the nature of the grain boundaries via mechanisms such as precipitation of secondary phases on and adjacent to the grain boundaries. A more likely explanation, however, is that the aging of the material is changing the resistance of the material and thus affecting the voltage measurement through the specimen over long periods of time. Given that the crack growth measurement is based on the voltage measured in the DC potential drop system, increasing inaccuracies in the crack length may have arisen during testing. The authors are further aware that the K parameter used to control the load during the test is only valid under elastic conditions. However, the stress intensity is merely used to define the load at the beginning of the curve since the K parameter obviously becomes invalid under creep crack growth conditions. The actual applied load for the duration of these quasi-static loading tests decreases only a small amount over a period of 1000+ hours. Under these considerations, the stress intensity parameter K is mostly likely valid for very short times at the beginning of the quasi-static loading period. Soon after the load is applied, a small creep zone forms at the crack tip and then grows with time, eventually invalidating K as the crack tip parameter. This evolution of the crack tip creep zone would also offer an explanation as to the increase in crack growth rate with time.

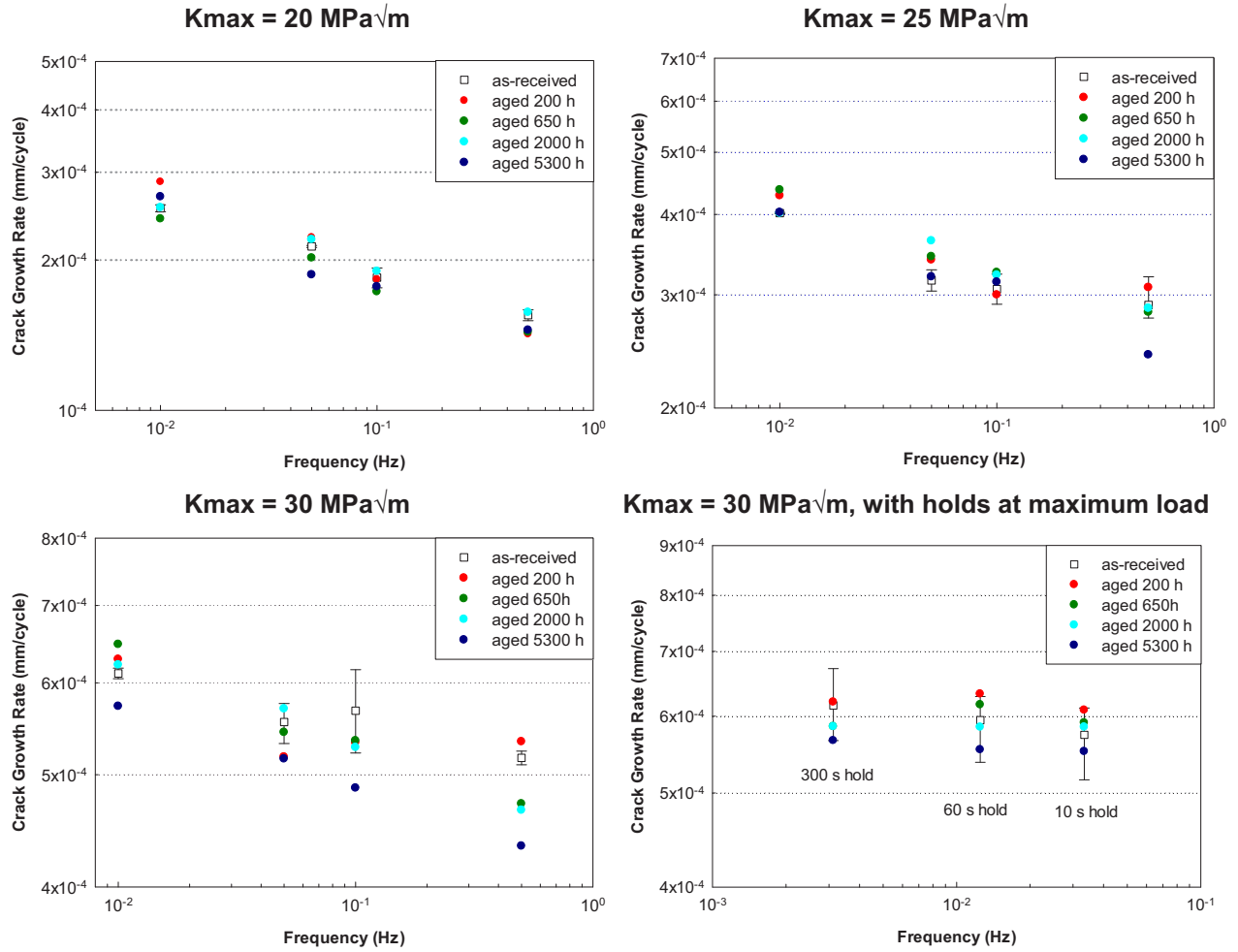


Figure 19. Plots comparing the crack growth rates vs. frequency for the as-received material and four aging times at 650°C. The data in each plot was generated under fatigue crack growth conditions at constant maximum stress intensity (K_{max}).

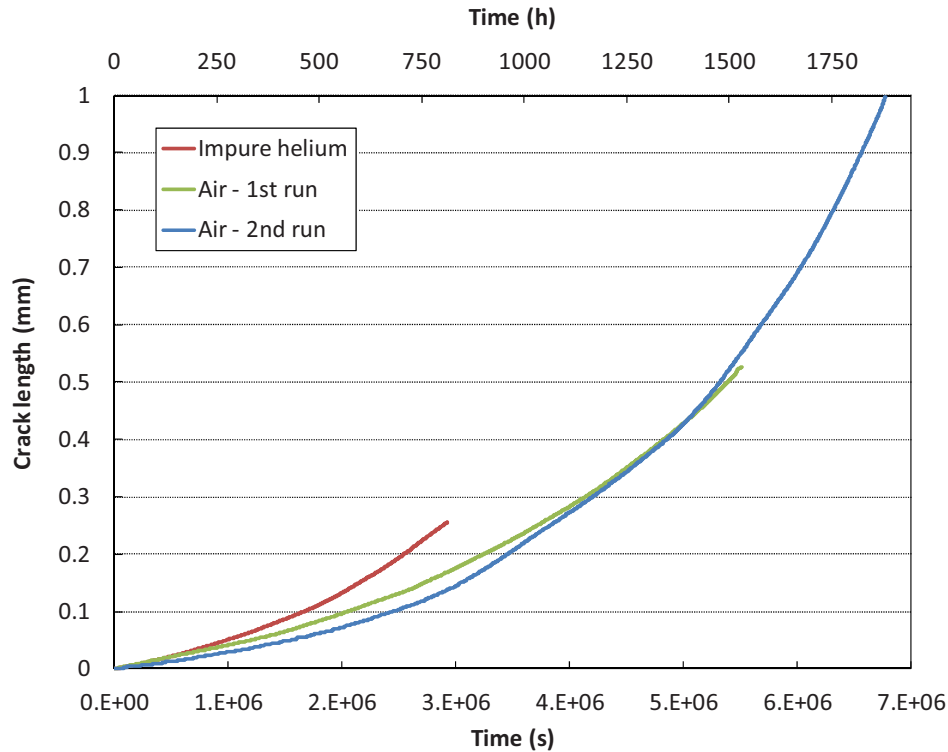


Figure 20. Crack length vs. time for compact tension specimens tested under quasi static loading conditions at $K = 40 \text{ MPa}\sqrt{\text{m}}$.

Gamma Prime Particle Size Analysis

Although the aluminum content of Alloy 617 is quite low, the presence of γ' (Ni_3Al) has been reported in material exposed to temperatures below 800°C .¹¹⁻¹³ Thermodynamic calculations by Ren, et. al., indicate the volume fraction of gamma prime should be quite low ($>5\%$ by weight) at 650°C .¹⁴ However, their calculations also indicated that γ' is unstable above about 650°C and that γ' observed above this temperature would eventually dissolve into the matrix at long aging times. In the present work, precipitation of γ' and interaction with dislocations during creep has been regularly observed as shown in Figure 21. In this figure, the dislocation density is relatively high compared to other creep samples tested at higher temperatures ($\geq 800^\circ\text{C}$) where γ' was absent and to similar total creep strains. The particles in creep samples tested at 750°C are very small ($\ll 100 \text{ nm}$) and, from the dislocation/particle interaction shown in Figure 21, could affect the time dependent deformation properties, e.g. creep and creep fatigue. Therefore, an analysis was carried out to understand the evolution and stability of the gamma prime particles in Alloy 617.

Materials Analyzed

Samples of material that were statically aged in a box furnace in air at 650 and 750°C for 200, 650, 2000 and 5300 hours were characterized. Additionally, one sample was aged at 750°C for 20,000 hrs. Analyses also were performed on interrupted creep test samples that were carried out at 750°C . Figure 22 shows the location of samples taken from the 750°C creep specimens and can be described as the shoulder area of the creep specimen. During creep testing, the extensometer is attached at a shallow groove in this shoulder area and the pull rods thread onto the ends of the creep specimen which is very near the shoulder area. Therefore, the temperature in this region may be slightly lower than that measured

by the Type R thermocouples attached in the gage section of the samples. Comparison to samples of material statically aged at 650°C and 750°C in a box furnace allow estimation of the actual temperature in the shoulder area of the interrupted creep samples to be made using an Arrhenius-type analysis.

Slabs of material were cut using a slow speed saw parallel to the rolling direction from both the statically-aged material and the interrupted creep samples (where the rolling direction was parallel to the long axis of the creep specimen). These slabs of material, approximately 500 microns thick, were reduced to approximately 175 micron in thickness by mechanical grinding. TEM blanks were punched from the thinned material and electropolished using ethanol-15% perchloric acid at 0°C and 34 volts. In the TEM, matrix grains were found that had an orientation close to the $\langle 111 \rangle$ zone axis and the gamma prime particles were imaged in dark field using a $\{110\}$ type superlattice reflection of the gamma prime so only the gamma prime particles appeared in the dark field images as shown in Figure 23. The extreme contrast afforded by darkfield TEM made it easy to analyze the γ' precipitates using image analysis. The particle diameter was analyzed using the image analysis program, AxioVS40, version 4.8.2, by Carl Zeiss MicroImaging, GmbH. A sufficient number of areas of view were acquired to ensure analysis of over 1000 particles for each aging temperature and time. In general, areas of view from multiple grains and multiple samples of each condition were analyzed.

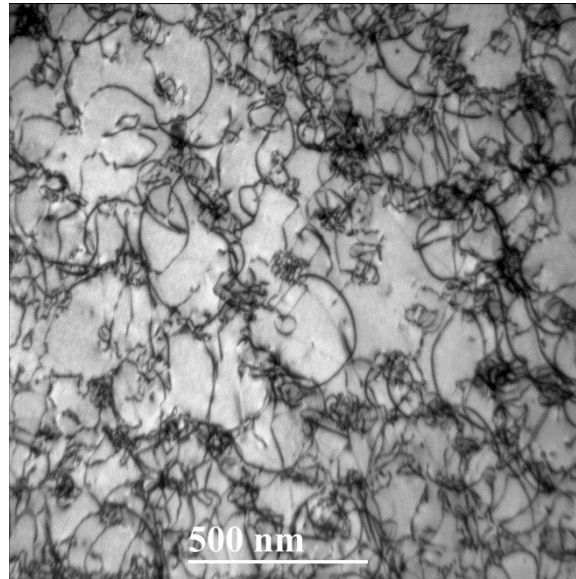


Figure 21. Bright field TEM micrograph showing interaction of γ' particles with mobile dislocations during creep at 750°C and 145 MPa, ~10% strain, 2127 hrs.

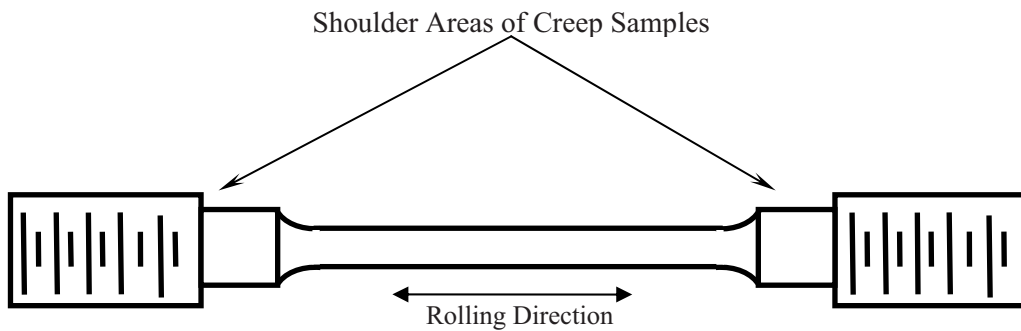


Figure 22. Schematic drawing showing the "shoulder" areas where TEM samples were taken for γ' particle size analysis.

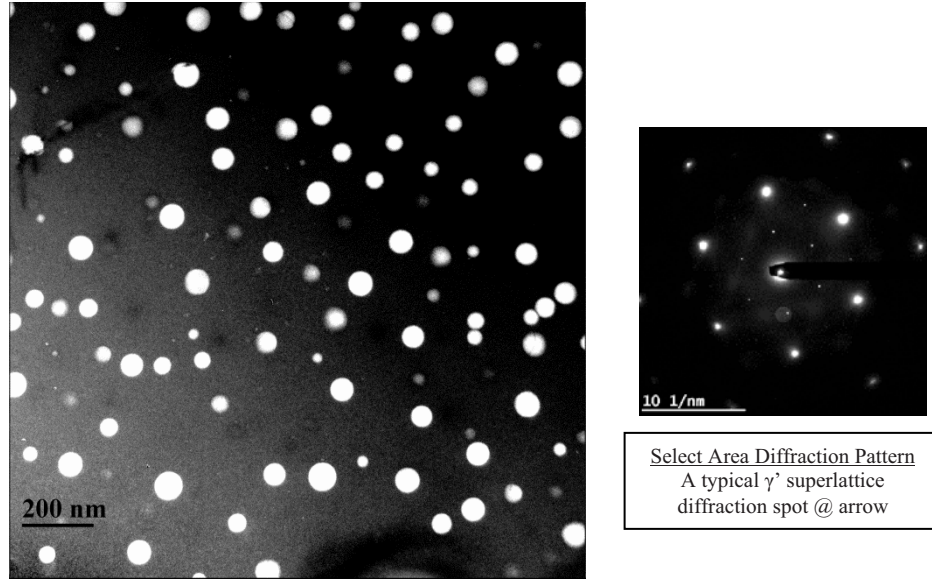


Figure 23. Dark field image (left) and the associated diffraction pattern (right) of I-617 statically aged at 750°C for 650 hrs.

Results and Discussion

The particle size distributions developed during static aging at 750°C are shown in Figure 24. As the aging time increases the distributions become broader and the average particle size increases. The behavior of the particle size distributions for the other datasets exhibited similar behavior. The main focus of the analysis, however, was to characterize the growth behavior of the gamma prime as a function of temperature so the influence of the gamma prime particles during high temperature deformation can be assessed. Figure 25 plots the average radius of the gamma prime particles as a function of aging time. A power law fit has been applied to each dataset and it is found that the radius follows a time to the 1/3 power relationship quite well for the static aged materials. This is in agreement with the coarsening model put forth by Lifshitz and Slyozov¹⁵ which is generally expressed as:

$$(\bar{r})^3 - r_o^3 = kt \quad \text{Eqn. (1)}$$

where

\bar{r} = average γ' particle radius

r_o = radius of the γ' particle at the onset of coarsening

k = growth rate constant

t = time

And plotting the average radius cubed as a function of aging time yields linear relationships for all three datasets (Figure 26). This relationship of r^3 has been found by a number of other researchers¹⁶⁻¹⁹ for coarsening of γ' in a variety of Ni-Al binary alloys and appears to be applicable to more complicated alloys. From the data in Figure 26 one can determine the growth rate constant, k , and the average initial particle radius, r_o , and is summarized in Table 5.

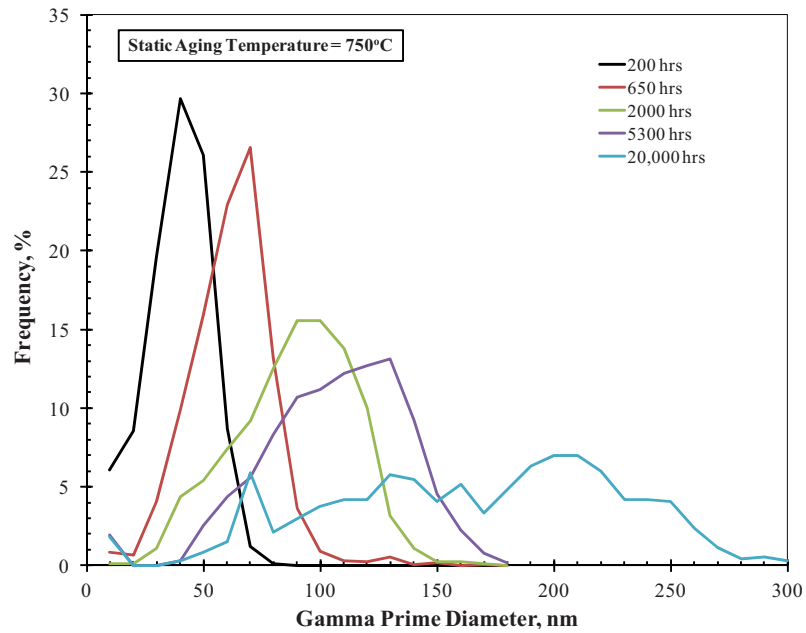


Figure 24. Gamma prime particle size distribution as a function of static aging time at 750°C.

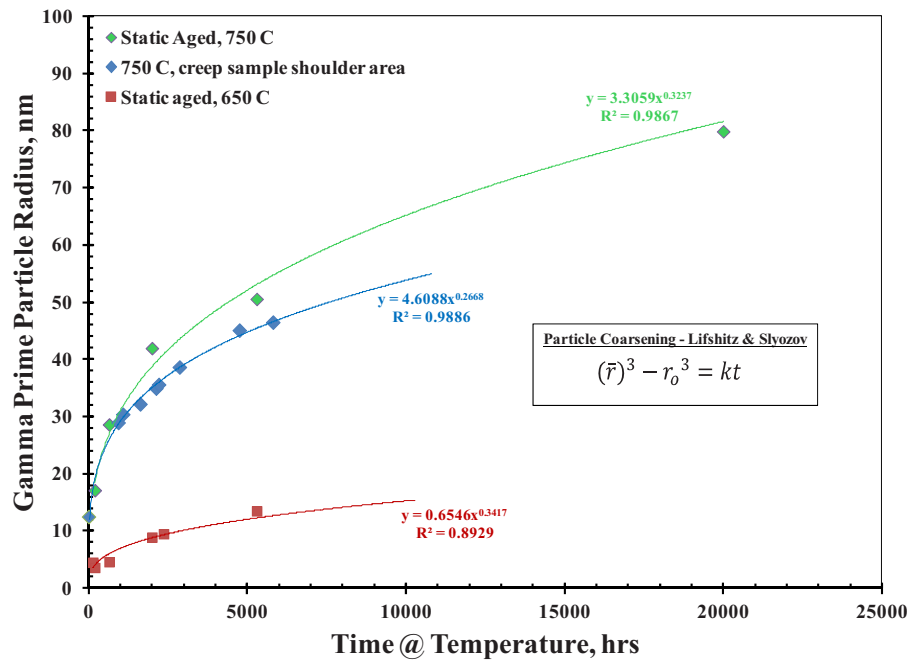


Figure 25. Plot of the average particle radius as a function of aging time.

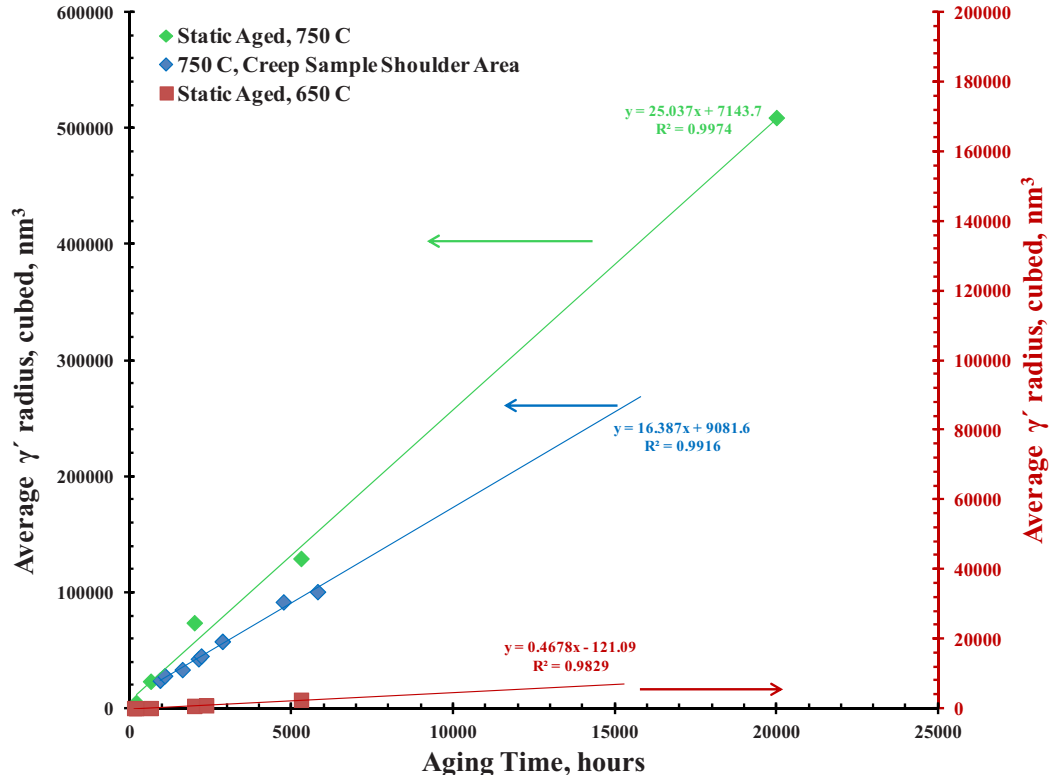


Figure 26. Plot of the cube of the average particle radius as a function of aging time.

Table 5. Growth Rate Constants.

Aging Condition	Growth Rate Constant, k (nm ³ /hr)	Initial particle radius, r_0 (nm)
Static Aging @ 750°C	25.0	19.3
Interrupted Creep @ 750°C	16.4	20.9
Static Aging @ 650°C	0.5	-5.0*

*This is essentially zero and the negative value is likely due to curve fitting errors.

The growth rate constant, k, has been shown to consist of the following¹⁷:

$$k = \frac{8\gamma D_{Eff} c_e V_m^2}{9RT} \quad \text{Eqn. (2)}$$

Where

γ = interfacial energy between γ' and the matrix

D_{Eff} = Effective diffusion coefficient

c_e = Equilibrium aluminum concentration in the matrix

V_M = Molar volume of the precipitate

Ultimately, it would be desirable to predict the growth rate constant at a specified aging temperature (or temperature of operation) to obtain the coarsening behavior of γ' and ultimately determine the influence (or lack of influence) of γ' on time-dependent deformation behavior. Both D_{Eff} and c_e in Eqn. (2) are exponentially temperature dependent.²⁰ However, to a first approximation:

$$c_e = A \exp(-Q_{\text{therm}}/RT) \quad \text{Eqn. (2a)}$$

and

$$D_{\text{Eff}} = D_o \exp(-Q_{\text{Diff}}/RT) \quad \text{Eqn. (2b)}$$

Then Eqn. (2) can be rewritten in the form:

$$k = A' \exp(-Q_{\text{Eff}}/RT) \quad \text{Eqn. (4)}$$

where A' contains the temperature insensitive constants and Q_{Eff} is the sum of $(Q_{\text{therm}} + Q_{\text{Diff}})$. Taking the natural logarithm of both sides of Eqn. (4) yields:

$$\ln k = -Q_{\text{Eff}} / R * 1/T + \ln A' \quad \text{Eqn. (5)}$$

Figure 27 shows the results of plotting $\ln k$ vs. $1/T$. Eqn. (5) implies a linear fit to the data, however, an additional aging temperature would help confirm this relationship. Assuming a linear fit, the growth rate constant for the data obtained from the creep samples tested at 750°C implies a temperature in the shoulder area of the creep sample (where the γ' particle size was determined) of approximately 738°C, as shown in Figure 27 by the red dotted lines. This seems reasonable since this area is near the attachment of the extensometer and the threaded pull rod, both of which will conduct heat away from this area and result in a temperature lower than that measured in the gage section of the creep specimen. In the future a thermocouple may be attached to a creep specimen in this area to verify the temperature in this location.

With the above analysis complete it is possible to predict the γ' particle size at very long aging times. Table 6 shows the estimated γ' particle size after 100,000 hrs at 650 and 750°C. It is likely that the contribution of γ' to the creep strength after 100,000 hrs will be minimal as the particles have grown to about 280 nm in diameter. However, at 650°C the γ' particles remain below 100 nm in diameter and are likely to continue to provide a significant contribution to the creep strength even beyond 100,000 hrs. However, the effect of stress and dislocation interaction (and potential dislocation pipe diffusion) on the growth the γ' particles has not yet been evaluated. Furthermore, it is not known whether γ' is thermodynamically stable at aging temperatures above about 600°C. Wu, et. al., did not observe any γ' after aging at 704°C and 43,000 hrs.¹³ Also, the ThermoCal calculation performed by Ren, et.al., indicates that γ' is unstable above about 650°C and eventually dissolves into the matrix above this temperature for the ASTM standard specification chemistry for Alloy 617.¹⁴ However, in their controlled chemistry alloy (CCA-617), γ' persisted to around 800°C. The heat of Alloy 617 under study in this program also appears to show persistent γ' at 750°C and 20,000 hours. Therefore, the influence of γ' on time-dependent deformation behavior at temperatures below about 800°C is likely to be very sensitive to alloy chemistry.

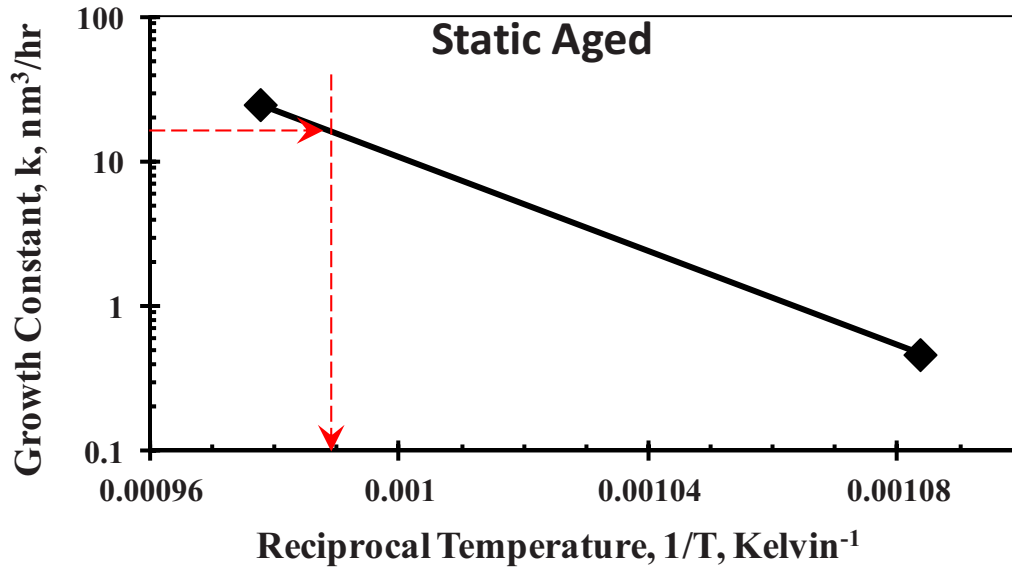


Figure 27. Plot of the γ' growth constant, k , versus reciprocal temperature. The grow rate constant for the data obtain from the 750°C creep tests yields a temperature in the shoulder region of the creep specimen of approximately 738°C.

Table 6. Estimated γ' Particle Radius after 100,000 hours.

Aging Temperature (°C)	Estimated γ' particle radius (nm)
750	140
650	35

Analysis of Creep Properties

A Zener-Hollaman fit to all of the creep data for the Alloy 617 plate characterized in this study is shown in Figure 28.²¹ It is apparent that data for the three higher creep temperatures fit on the same regression line, indicating that the creep behavior is characterized by a single Norton equation:

$$\dot{\epsilon} = A\sigma^n e^{-Q/RT} \quad \text{Eqn. (6)}$$

The data for creep at 750°C appears from this plot to exhibit a common slope, indicative of a single stress exponent. The offset on the stress axis indicates that there is a different apparent activation energy. It is known from the transmission electron microscopy shown above that there is a significant volume fraction of γ' formed at this temperature. This phase is not formed at the higher aging or creep temperatures.

It is reasonable to assume that the formation of this phase contributes to enhanced creep resistance through a threshold stress mechanism:

$$\dot{\epsilon} = A(\sigma_{\text{applied}} - \sigma_{\text{threshold}})^n e^{-Q/RT} \quad \text{Eqn. (7)}$$

Figure 29 shows the conventional method of presenting the creep data used to extract a value for the threshold stress.²² Extrapolation to zero strain rate gives the value for the threshold stress. It can be seen from the plot that there is a threshold stress of 65MPa for the 750°C creep properties. At the higher

temperatures there is no evidence for a threshold stress. This observation is consistent with the lack of γ' in samples above 750°C examined using TEM.

The observation here of increased creep strength associated with γ' formation is in accord with results for the modified CCA 617 alloy developed for fossil energy applications.²³ This alloy has specific increases in the Al and Ti content intended to increase the volume fraction of γ' for application in the temperature range from 600 to 750°C. It has been shown that the creep rupture properties of CCA 617 are superior to conventional Alloy 617 below 750°C; above that temperature the rupture lives are comparable.²³

If the value of 65 MPa for the threshold stress is used to correct the applied stress for creep at 750°C a new Zener-Hollaman plot can be developed as shown in Figure 30. After application of the threshold stress it is evident that all of the creep data fall on a single line with a stress exponent of 5.7 and an activation energy of approximately 400KJ/mole.

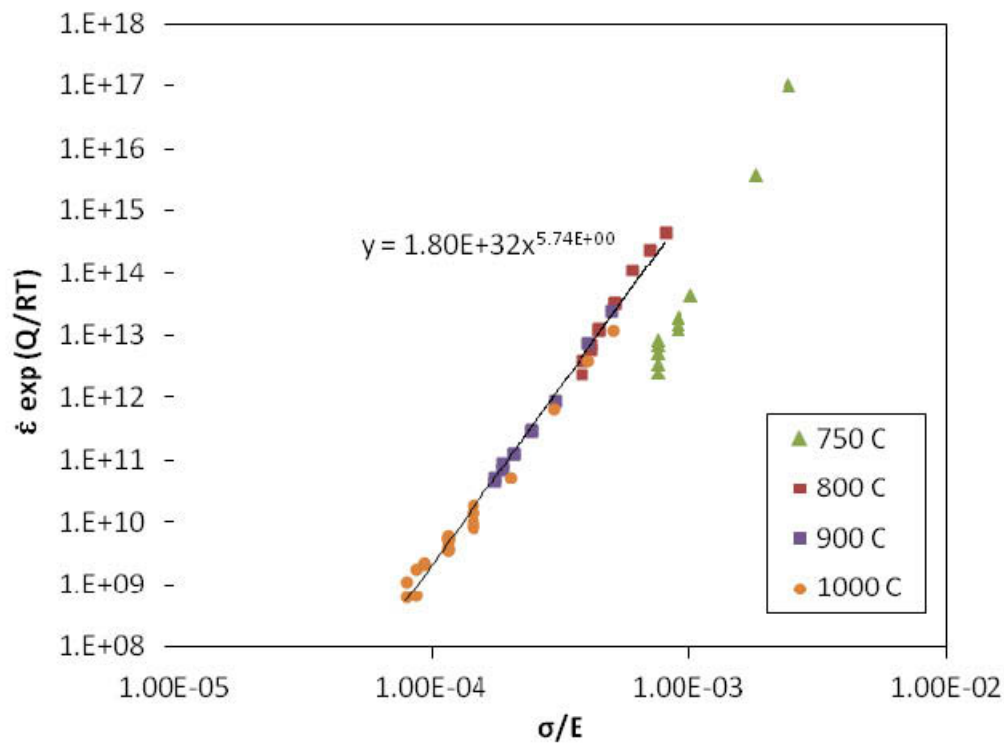


Figure 28. Zener-Hollaman type plot for creep of Alloy 617.

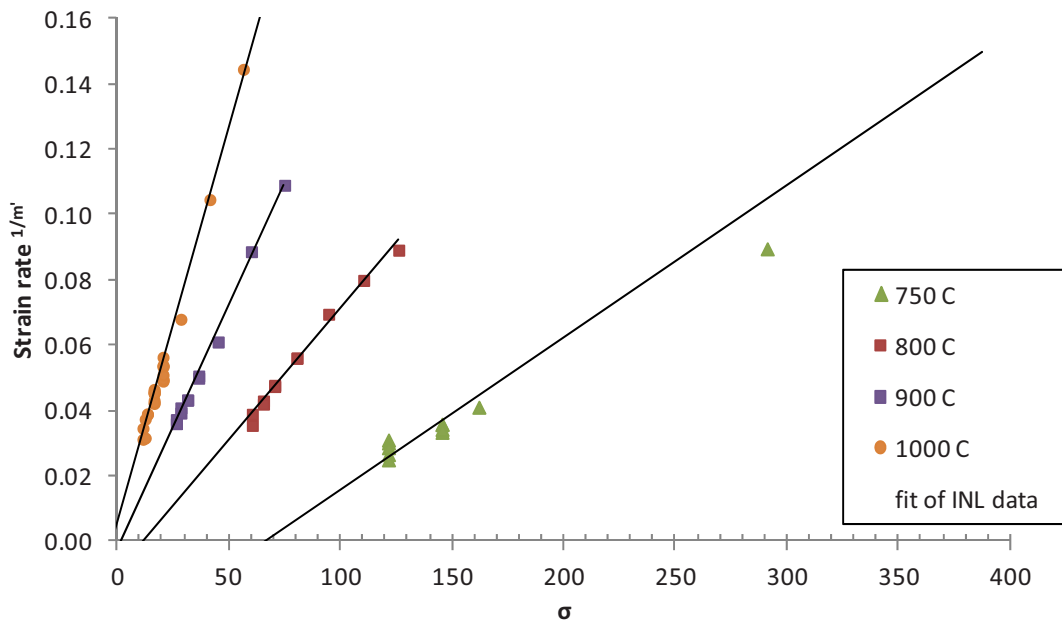


Figure 29. Linear plot of strain rate to the 1/m power plotted against stress, from which the threshold stress can be determined.

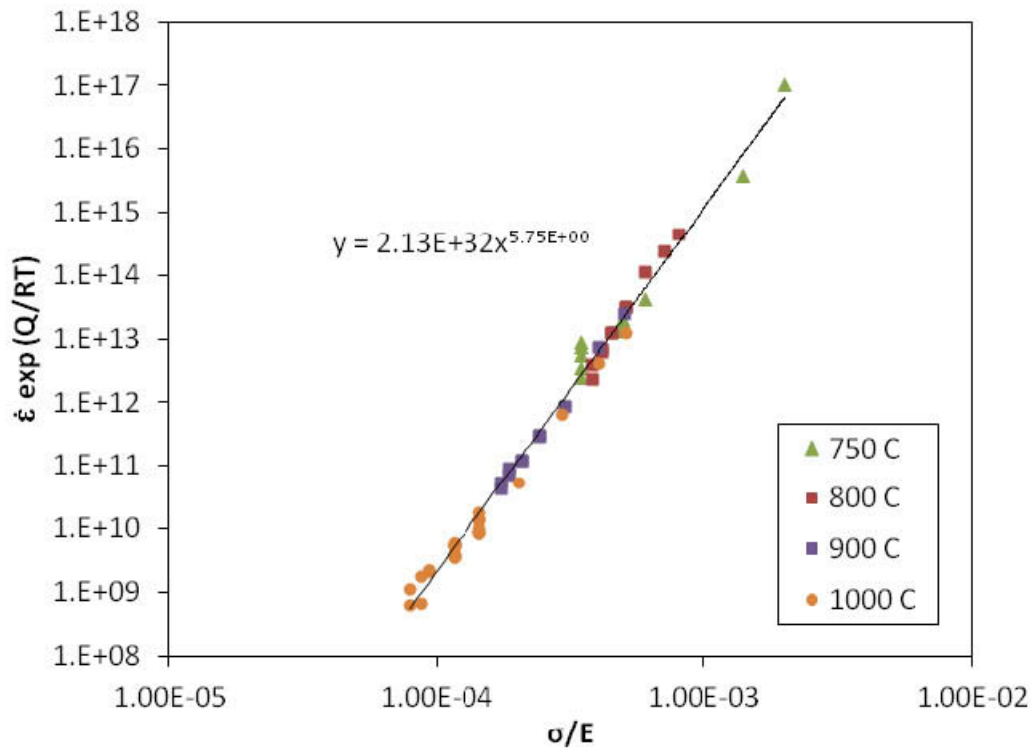


Figure 30. Zener-Hollaman type plot for Alloy 617 creep data with a threshold stress of 65 MPa applied to the data for 750°C.

CONCLUSIONS

Alloy 617 has been aged at 650°C for times up to 5300 hours. The microstructure after aging has been characterized using optical and transmission electron microscopy (TEM). The Alloy 617 plate shows an evolution of microstructure even after aging for relatively short period of 200 hours at both 650 and 750°C. This observation is consistent with the TTT diagram for Alloy 617 which shows that $M_{23}C_6$, M_6C , and γ' will start precipitating in as little as one hour at these temperatures. Comparing the as-received microstructure to that of aged material, both the 650 and 750°C show a similar amount of carbide precipitation. At both aging temperatures, the majority of carbides are intragranular and there is no indication of carbide redistribution or precipitation directly on the grain boundaries. The carbides appear to partly retain the cell structure seen in the as-received material in the banding regions. It has been determined that in addition to carbides, a significant volume fraction of γ' phase (Ni_3Al,Ti) is formed at these temperatures. The $Ni_3(Al,Ti)$ phase is only observable using TEM. The size and morphology of the carbides and γ' continue to evolve with increasing aging time at both temperatures.

After aging at 650°C the room temperature yield and tensile strength increase with increasing time. The ductility decreases from 62% in the solution annealed material compared to 42% for material aged for 5300 hours. Aging has a more significant influence on the impact properties of Alloy 617 compared to the tensile properties. The room temperature Charpy energy for the solution annealed Alloy 617 is above 150J. Aging for 200 hours results in a decrease in Charpy energy to 95J and 75J for aging at 750 and 650°C, respectively. Increasing the aging time to 5300 hours at 650°C results in a further reduction in Charpy energy to approximately 60J.

Precipitation and coarsening kinetics of γ' has been studied in detail after aging at both 650 and 750°C. It has been found that the presence of this phase affects the creep properties of Alloy 617 at 750°C. A threshold stress model is necessary to account for the creep behavior at this temperature, with a value for $\sigma_{\text{threshold}}$ of approximately 65MPa. Above this temperature there is no formation of γ' and the creep properties can be modeled with a conventional Norton Law formulation with no threshold stress.

References

1. Ren W. and Swindeman R., "Preliminary Consideration of Alloys 617 and 230 for Generation IV Nuclear Reactor Applications," Proceedings of the 2007 ASME Pressure Vessels and Piping Division Conference, San Antonio, TX, July 22-26, 2007.
2. B 168 - 08, Standard Specification for Nickel-Chromium-Iron Alloys (UNS N06600, N06601, N06603, N06690, N06693, N06025, N06045, and N06696) and Nickel-Chromium Cobalt Molybdenum Alloy (UNS N06617) Plate, Sheet, and Strip, ASTM International, 2008.
3. Wu, Q., Hyojin, S., Swinderman, R.W., Shingledecker, J.P., Vasudevan, V.K., "Microstructure of Long-Term Aged IN617 Ni-Base Superalloy," *Metallurgical and Materials Transactions*, **39A**, 2008, pp. 2569-2585.
4. Krompholz K., et al., "Determination of J-Integral R-Curves for Hastelloy X and Inconel 617 up to 1223K Using the Potential Drop Technique," *Werkstofftech.*, Vol. 13, 1982, p. 236-244.
5. Clarke G. A., et al., "A Procedure for Determination of Ductile Fracture Toughness Values Using J-Integral Techniques," *Journal of Testing and Evaluation*, Vol. 7, 1979, p. 49-56.
6. Landes J. D. and Begley J. A., ASTM, Test Results from J-Integral Studies; an Attempt to Establish a JIC Testing Procedure; STP 560.
7. Bassford T. H. and Schill T. V., "A Review of Inconel Alloy 617 and Its Properties after Long-Time Exposure to Intermediate Temperatures," *Applications of Materials for Pressure Vessels and Piping*, Smith G. V., Ed. ASME: 1979; Vol. MPC-10, p. 1-12.
8. Bruch U., et al., "Tensile and Impact Properties of Candidate Alloys for High-Temperature Gas-Cooled Reactor Applications," *Nuclear Technology*, Vol. 66, 1984, p. 357-362.
9. Mankins, W. L., Hosier, J. C. and Bassford, T. H., "Microstructure and Phase Stability of INCONEL Alloy 617," *Metallurgical Transactions*, **5**, pp. 2579-2590, 1974.
10. Rabin, B.H., Swank, W.D. and Wright, R.N., "Thermophysical Properties of Alloy 617 from 25 to 1000°C," submitted to *Nuclear Engineering and Design Journal*.
11. Kimball, G. F., Lai, G. Y. and Reynolds, G. H., "Effects of Thermal Aging on Microstructural and Mechanical Properties of a Commercial Ni-Cr-Co-Mo Alloy (Inconel 617)," *Metallurgical Transactions*, **7A**, pp. 1951-1952, 1976.
12. Kirchhofer, H., Schubert, F. and Nickel, H., "Precipitation Behavior of Ni-Cr-22Fe-18Mo (Hastelloy X) and Ni-Cr-2Co-12Mo (Inconel 617) after Isothermal Aging", *Nuclear Technology*, **66**, pp. 139-148, 1984.
13. Wu, Q. and Vasudevan, V. K., "Characterization of Boiler Materials for Ultracritical Coal Power Plants," *Annual Progress Report for Period August 1, 2002 to July 30, 2003* under UT-Battelle Sub Contract Number 4000017043, 2004.
14. Ren, W. and Swindeman, R., "Development of a Controlled Chemistry Specification for Alloy 617 for Nuclear Applications", ORNL/TM-2005/504.
15. Lifshitz, I.M. and Slyozov, V.V., "The Kinetics of Precipitation From Supersaturated Solid Solutions", *J. Phys. Chem. Solids*, vol. 19, 1961, pp. 35-50.
16. Ardell, A.J. and Nicholson, R.B., "The Coarsening of γ' in Ni-Al Alloys", *J. Phys. Chem. Solids*, vol. 27, 1966, pp. 1793-1804.

17. Ardell, A.J., "An Application of the Theory of Particle Coarsening: The γ' Precipitate in Ni-Al Alloys", *Acta Met.*, vol. 16, 1968, pp. 511-516.
18. Ro, H. and Mitchell, T.E., *Met. Trans. A*, vol. 9A, 1978, pp. 1749-1760.
19. Jung, P., Ansari, M.I., Klein, H. and Meertens, D., "Diffusion and γ' -Precipitation in Ni(Al) Alloys Under Proton Irradiation", *J. Nuc. Matls.*, vol. 148, 1987, pp. 148-156.
20. Porter, D.A and Easterling, K.E., *Phase Transformations in Metals and Alloys*, Van Nostrand Reinhold (UK) Co, LTD., 1981, p. 314-317.
21. Sherby, O. D., and Burke, P. M., "Mechanical Behavior of Crystalline solids at Elevated Temperature", *Progress in Materials Science*, vol 22, 1982, pp. 325-390.
22. Hedworth, J. and Stowell, M. J., "The Measurement of Strain Rate Sensitivity in Superplastic Alloys", *Journal of Materials Science*, 1971, Vol. 6, pp. 1061-1069.
23. Viswanathan, R., Purgert, R., Goodstine, S., Tanzosh, J., Stanko, G., and Shingledecker, J. P., "U.S. Program on Materials Technology for Ultrasupercritical Coal-Fired Boilers", *Advances in Materials Technology for Fossil Power Plants: Proceedings of the 5th International Conference*, ASM International, 2008.